1-1-1981

Measurements of liquid film dynamics in air-water counter flow.

Sau-To Lau

MEASUREMENTS OF LIQUID FILM DYNAMICS IN AIR-WATER COUNTER FLOW

by

Sau-To Lau

A Thesis

Presented to the Graduate Committee

of Lehigh University

in Candidacy for the Degree of

Master of Science in Mechanical Engineering

Lehigh University

1981

This thesis is accepted and approved in partial fulfillment of the requirements for the degree of Master of Science.

May 4, 1981
(date)

Professor in Charge

Chairman of the Department

Acknowledgements

Throughout the course of this work I received most valuable guidance and encouragement from my thesis advisors, Dr. Ramu K. Sundaram and Professor John C. Chen to whom I wish to express my gratitude.

TABLE OF CONTENTS

LIST OF FIGURES

LIST OF TABLES

Nomenclature

ω_L	liquid mass flow rate
ρ_L	liquid density
g	acceleration due to body force
L	periphery width
δ	film thickness
μ_L	liquid viscosity
Γ	liquid flow rate/unit channel periphery
η	magnitude of the universal distance parameter at the liquid surface
u+	dimensionless velocity (u/u_*)
u	local film velocity
u_*	friction velocity $(\tau\omega/\rho_L)^{\frac{1}{2}}$
$\tau\omega$	wall shear
y+	dimensionless distance $(u_*\rho_L y)/\mu_L$
y	distance from the wall
c	capacitance
ϵ_r	dielectric constant
d	distance between electrodes
Q_L(QL)	liquid feed rate
J_A(JA)	air velocity
Q_D(QD)	drainage rate
P	pressure
z	axial distance or coordinate

τ_i	shear stress at the interface
Q_F(QF)	approximate local film flow rate
Vg^*	dimensionless gas flux
Vg	superficial gas velocity
ρ_g	gas density
D	equivalent tube diameter
$V\ell^*$	dimensionless liquid flux
$V\ell$	superficial liquid velocity

Abstract

An experimental investigation of counter-current air-water flow in a vertical annulus has been conducted. Specially developed capacitance probes were used to measure the average and localized film thickness of downward flowing film at various water and air flow rates. The results were found to be consistent with current theory on liquid film dynamics. The flooding point was predicted well by the Wallis correlation [19]. A previously developed probe for local measurement of film flow rates (EP probe) was tested in the presence of interfacial shear and calibration data obtained. In addition, integral measurements of liquid entrainment have been made and yield useful information on carry-over rates. Photographs of the capacitance probe signal traces have also been obtained and provide a visual description of the film surface at various water and air flow rates.

1. Introduction

There are numerous practical applications for which it is necessary to have understanding of two-phase countercurrent flow. This type of flow pattern would be expected to occur in industrial process equipment such as wetted-wall columns, vertical condensers, water tube boilers, etc. The stimulus for the present investigation came from the work concerned with the flow of coolant in the core shroud, rod bundles and upper plenum of water-cooled nuclear reactors during loss-of-coolant accidents (LOCA). Information on amount of liquid hold-up, entrainment, and gas-liquid interactions are important to the analysis of system behavior.

1.1 Previous Work

In analysis of liquid film dynamics, the major parameters are the film thickness, film flow rate and the interfacial shear rates at the boundary surface of the film. The relationship between these parameters can be established in such a way that for a given velocity profile in the liquid film it is possible to predict one of these quantities from a knowledge of the other two. In addition, in counter-flow shear situations, film surface behavior is important. Wavy surfaces can generate roll waves and possible bulk shearing of liquid from the film.

Previous investigators have attempted to describe these phenomena by various methods.

1.1.1 Liquid film in free flow

The earliest descriptions of free film behavior was presented by Nusselt. His equations, derived from force balance on an element in the liquid film, were based on the assumption of viscous flow with no interfacial shear. In vertical, planar geometry, the film thickness and liquid mass flow rate are related by:

$$\omega_L = \frac{\rho_L^2 g L \delta^3}{3\mu_L} \quad . \tag{1.1}$$

Kirkbride [1] used a micrometer to measure the film thickness on the outside surface of a cylindrical rod. Disagreements of data with Nusselt's theory were found and these disagreements were hypothesized to be due to ripples on the film surface. However, good agreement of film thickness data with Nusselt's theory was observed by Jackson [2] in his experiments in an annular geometry even though waves were present on the film surface. A more reliable technique, using radioactive tracers, was employed by Jackson for film thickness measurement.

In turbulent flow, the velocity profile is different from the laminar case. Dukler and Bergelin [3] assumed that the

von Karman universal velocity profile [4] was applicable in the film and derived an expression for the liquid mass flow rate per unit length of wetted periphery as:

$$\frac{\Gamma}{\mu_L} = 3.0\eta + 2.5\eta \ln \eta - 64 \tag{1.2}$$

where

$$\eta = \frac{\rho_L g^{\frac{1}{2}} \delta^{3/2}}{\mu_L} \cdot \tag{1.3}$$

It was suggested [3] that equation (1.2) can be applied in laminar, buffer and turbulent regions of film flow. Experimental data on film thickness from Dukler and Bergelin seem to confirm their analytical work. Portalski [5] compared his film thickness data obtained by a hold-up technique with both Nusselt's and Dukler-Bergelin theory and concluded that good agreement with data was obtained for turbulent films with the universal velocity profile approach. All these analyses apply for film flow with no interfacial shear at the free surface.

1.1.2 Film flow with interfacial shear

In analyzing film flow in the presence of substantial interfacial shear, Anderson and Mantzouranis [6], using the universal velocity profile of von Karman, established an implicit expression between film thickness, film flow rate, and

frictional pressure drop in a cocurrent upward annular flow. The theory seems to predict a wide range of experimental data. However, experiments by Collier and Hewitt [7] show that Anderson and Mantzouranis analysis under predicts the film flow rate at low wall shear and overpredicts the film flow rate at higher wall shear. Since the universal velocity profile is based on a constant shear stress across the film, they imposed a shear stress correction factor on the method proposed by Anderson and Mantzouranis. This yielded better agreement with data.

Dukler [8] later published a more sophisticated method for the analysis of co-current liquid-gas flows, based on the use of the Deissler expression for the eddy viscosity near the wall. The method accounts for interfacial shear at the gas-liquid interface, but does not provide an analytical solution. Dukler has suggested a graphical/numerical procedure for obtaining a solution. Film thickness data of a co-current downward flow obtained by Charvonia [9] have been compared by Kosky [10] to Dukler's predictions, and good agreement was observed. For ease of calculations, Davis [11] used a less generally acceptable expression for the eddy viscosity to obtain an explicit solution which related liquid flow rate to film thickness, pressure drop and wall shear stress. Only

low value of interfacial shear data were compared, disagreements with the theory were found and was hypothesized to be due to the wavy surface of the liquid film.

Kosky [10] used a two region approximation in the liquid film - u+=y+ near the wall and Prandtl's 1/7th power law for the outer region, together with a wall shear and interfacial shear relation developed by Rohsenow et al. [12]. The liquid flow rate was related to the dimensionless film thickness (which included the shear stress terms) by integrating across the two regions. Even though the resulting equations were simple to apply, his comparison with others experimental data shows that accuracy of prediction is largely sacrificed.

1.1.3 Flooding

Most of the studies described above are for either co-current upward or co-current downward flow. A few studies have been found in the literature dealing with counter-current flow and some of these studies have looked at the flooding phenomena [13-19]. In counter-current flow several regimes of flow occur which are a function of the gas and liquid flow rates. These regimes can be observed sequentially as the gas flow rate is increased at a constant liquid flow rate. A free falling film is formed when no gas is flowing upward. With increasing gas

flow rates, the film surface becomes rough and wavy because of significant interaction between the gas and liquid flows. With further increase in gas rate, the flow becomes chaotic, and a regime is expected to exist where both falling and climbing film flow occur simultaneously. A flooding point is said to be reached when the liquid can no longer flow downward. Thus, flooding is the limit condition for counter-current flow. Most of the experimental studies of flooding [13-16] were for flow inside of tubes. Recently, Blass [20] gave a review of counter-current flow in vertical tubes and showed a comparison of his free film data with the Dukler and Bergelin theory.

1.2 Scope of Present Study

As mentioned earlier, several investigations have been done on co-current flows and flooding, but only limited data have been found on counter-current flow, especially flows on the surface of cylindrical rods such as those encountered in fuel bundles and upper plenums of nuclear reactors. This lack was partly due to limitations of the film measurement techniques.

The present investigation was undertaken to (a) develop and calibrate improved instrumentation for measurement of both film thickness and film flow rates, and (b) use these improved instruments to characterize counter-current gas/liquid flows up to the flooding limit.

2. EXPERIMENTAL APPARATUS

2.1 Technique for film thickness measurement

In two-phase flow experiments, there are a number of methods for measuring the film thickness, some of which have been mentioned in the previous chapter. A summary of these and other techniques can be found in references [18, 23-25].

Dukler and Bergelin [3] used the principle of capacitance between two electrodes, one of which was placed above the liquid surface and the other on the wall. In this parallel-plate type of capacitance probe, the measured capacitance would vary linearly with the film thickness. Tailby and Portalski [26] used the same principle, but with a smaller capacitance probe for wave profile measurement. Both of these techniques are incapable of measuring large fluctuation of film thickness and obstruct the gas stream.

In countercurrent film thickness measurement, it is desirable to have a non-intrusive probe which is both sensitive and responsive over a large range of film thickness. One probe which has these characteristics was developed at Lehigh University [21,22,27]. This capacitance probe consists of two conducting plates placed flush with the surface over which the liquid film flows. The capacitance of these condenser plates is proportional to the dielectric constant of the thin liquid

film and the film thickness above the plates.

$$c = \varepsilon_r \cdot f_1(\delta,d)$$

For a given gap (d) between the conducting plates, $f_1(\delta,d)$ varies as the thickness of film above the plates changes. A consequence of this is that for a given probe geometry the change of capacitance of the probe can be directly related to the change of film thickness. The calibration of such a probe is discussed in the next chapter. It is possible to use this probe in such a manner that the liquid dielectric constant is not an important parameter. This is a particularly valuable asset.

The probe described above can be calibrated to be sensitive for any film thickness by changing the geometry. In the present study, special capacitance probes with different geometries were built on a rod surface which could be inserted in the main test rig (described later) and form an integral part of the test column. Figure 1 shows a band probe, which consists of two copper band electrodes 0.635 cm in width placed around the rod circumference. The gap between the electrodes was chosen to be equal to the width of the electrodes. It was shown that [22] if the film thickness is within half the width of the electrodes of the band probe, the capacitance of the probes is approximately linearly related to the film thickness. One distinct feature of this band probe is that it is capable of

measuring the instantaneous circumferentially integrated film thickness above its surface.

Figure 2 shows another type of capacitance probe (Split-D type). The probe consists of two "D" type electrodes separated by a gap of 0.6731 mm, and insulated from the plate ground by a distance of 3.0683 mm. The small size of this probe makes it useful to measure 'local' instantaneous values of film thickness. This probe can be used with two sets of electrode pairs - one between the two 'D_S' and the other between any one 'D' and the outer ground surface. As mentioned before, the gap between the electrodes determines the sensitive (linear) range of operation of the probe. Since the two electrode pairs have different gaps, one can choose the electrode pair to be used based on the magnitude of the expected film thickness. This option is one of the attractive features of this probe. The 'local' film thickness can also be tracked dynamically by transmitting the capacitance signal to an oscilloscope or strip-chart recorder. This allows the investigator to study the wave profile of the film.

A typical signal trace of capacitance values versus film thickness ($\Delta C/\Delta Cm^*$ vs. δ/d) is given in Figure 7. ΔC and ΔCm

*ΔC is defined as the capacitance between the two electrodes at any given film thickness δ. ΔCm is defined as the maximum capacitance between these two electrodes for 'very thick films'.

values were used in order to zero out air reading and to cancel out the dielectric constant. Probes with two gap sizes are shown in Figure 7, which have the same asymptotic value but slightly different sensitive ranges.

2.2 Electrolysis Potential Probe (EP Probe)

In study of film dynamics, data on local film flow rate or local film velocity is essential but difficult to obtain. Devices such as hot-wire anemometers or hot-film probes [24] both alter and obstruct the flow stream, and may not be applicable to geometries encountered in reactors. A non-intrusive type of probe which is capable of measuring wide ranges of local flow velocity and can be placed flush on a surface was developed at Lehigh University [22]. The Electrolysis Potential Probe (EP Probe) consists of two platinum wires, separated by a predetermined gap and placed longitudinally along the flow direction. For a constant applied D.C. potential, the variation of electrolysis current (which is proportional to the rate of electrolysis) with film velocity depends on the inherent electrical resistance across the electrodes (which is a function of electrode diameter, electrode length, distance between electrodes, electrical resisivity of the electrolyte, and the film thickness over the probe surface). A relationship between the electric

resistance, electrolysis current and film velocity can be obtained by suitable calibration [22].

In operation, a constant D.C. potential (usually about 100 volts) is supplied to the electrodes of the probe and the resultant d.c. current measured. In addition, the ohmic resistance (R_p) across the electrodes is also measured (in the absence of electrolysis) by an A.C. impedance bridge. It has been shown [22] that for a given applied voltage, the product of electrolysis current and ohmic resistance is dependent only on the film flow rate and film thickness. If the film thickness is measured independently (using capacitance probes, for example), the EP probe output can be calibrated for a range of film velocities. In previous tests of the EP probe [21,22], only bounded films and free films with no interfacial shear were used. It was suggested [22] that the velocity profile in the film could affect the EP probe response. Hence, it was decided to test the EP probe in films with large interfacial shear.

In the present study, two EP probes were mounted at the same axial location as the capacitance probes, each EP probe being displaced 90° with respect to each capacitance probe (see Figure 2). An EP probe consisted of two platinum wires, 0.251 mm in diameter, 23.622 mm long, separated by a gap of 0.884 mm. One EP probe was connected to a D.C. power supply

with a millimeter in series and the other EP probe was connected to an impedance bridge for simultaneous measurement of the ohmic resistance. The objective was to observe the behavior of the EP probes at conditions where the total film flow rate and the local film thickness were known. It was hoped that these tests would be able to generate calibration data for the EP probes in films with considerable interfacial shear.

2.3 Description of Counter-flow Air-water Rig

An experimental apparatus was designed and constructed to generate downward flowing liquid films with counterlfow air and to measure the pertinent flow rates and film thicknesses in a vertical annulus. The counter-flow air-water rig was mounted on a rigid supporting table and special care was taken to level the apparatus. A schematic diagram of experimental apparatus is shown in Figure 3.

The liquid was introduced onto the outside of the inner tube through the top by a 9.525 mm inner concentric soft plastic tube. The O.D. of the inner tube was 5.08 cm and the I.D. of the outer tube was 10.16 cm, and the total length of the tube was 1.83 m.

The inner tube was of aluminum and was assembled from several lengths of short tubes which were screwed together. It

was so designed such that the instrumented segment (containing band, split-D and EP probes) could be located at various axial positions relative to the film entrance. The top section was bevelled to elimate edge effects in liquid introduction. All the screwed sections were made flush with each other to avoid disturbance of the liquid film. The outer tube was made of plexiglass to allow visual observations. A specially designed spacer was installed at the top of the apparatus to keep the inner and outer tubes aligned without causing flow disturbances.

Air was introduced by ten (0.953 cm dia.) air injectors at the bottom of the test section, which in turn connected with the air distributor prior to entering the base of the test column. The air distributor was made from a 12.7 cm schedule 40 pipe nipple with capped ends. The inlet hole to the air distributor was 5.08 cm. A calming length of 0.9 m was allowed before the air reached the test section. Water was introduced through the top of the inner tube, flowed counter-current with the air and drained through three outlets at the bottom of the test column.

Water flow rates were monitored by using a rotameter (Shutte and Koerting, Model 3-HCFb, Float 32-J, 1.02×10^{-4} m^3/s max. flow rate), the rotameter was carefully calibrated by weight measurement and checked during the course of data

gathering. Air flow rates were monitored using a manometer which measured differential pressure across an orifice. The flow meter could handle up to 8.46×10^{-2} m^3/s of air flow. A pressure regulator (CASH ACME, TYPE E55) was used to maintain an upstream pressure of approximately 3.45×10^5 N/m^2 prior to the air flow meter, and air was supplied by a compressor of maximum capacity 0.236 m^3/s at a pressure of 6.89×10^5 N/m^2.

2.4 Experimental variables and their measurement

The parameters that were measured in this experiment were: liquid feed rate, Q_L, from the rotameter; air flow rate, Q_A, from the orifice meters; drainage rate, Q_D, by weight measurement of the discharged water; film thickness, δ, from capacitance measurement; the electroysis current, I, and ohmic resistance R_p of the EP probe. All measurement were carried out at ambient temperature and pressure.

Figure 4 shows pertinent measuring instruments and output recorders. Capacitance measurements were obtained with a one MHz digital capacitance bridge (Boonton Model 72BD, accuracy 0.25% of reading). The capacitance signal could be recorded on a strip-chart recorder or displayed on an oscilliscope. The strip-chart recorder with a special integrator (Esterline Angus, Speed Servo II Model 70D7) could record a time varying signal

as well as give a time-averaged mean value. The oscilloscope used was a Nicolet 1090A digital oscilloscope, in which the input signal could be retained and expanded on a vertical and horizontal scale for detailed study. A Polaroid camera was used to obtain permanent records of the signal.

A constant voltage of 100 volts was applied across the EP probe through an 'electronics module', the circuit diagram of which is given in Figure 5. This circuit was specially built for electrolysis measurements, and could simultaneously detect electrolysis current or ohmic resistance for two channels. The output, in terms of voltage, could be displayed and recorded on the digital oscilloscope and the strip-chart recorder.

All leads were shielded cables and these were properly grounded to avoid undesirable disturbance from the surroundings.

3- EXPERIMENTAL RESULTS

3.1 Calibration of Probes

3.1.1 Band Probe Calibration

Calibration of band probes were obtained using a horizontal trough (Figure 6). Two band probe sizes were chosen (0.508 cm and 0.635 cm in width), but only the 0.635 cm probe was used for data gathering. Copper strips with the same length of coverage on the test section were placed flush with the base of the trough. The capacitance bridge was employed for capacitance measurement. An accurate value of liquid depth could be obtained from volumetric measurements, and, together with the corresponding capacitance values, a calibration curve could be generated. Figure 7 shows the calibration of both band probes. All data including the 0.508 cm band probe can be found in table 1 in Appendix A. The lower portion (first 25 data points) of the 0.635 cm probe in Figure 7 were used to generate a third degree polynomial curve fit. This calibration equation relating normalized capacitance reading with film thickness was used later on all subsequent film thickness calculations.

3.1.2 Split-D probe Calibrations

The calibration of split-D probes presented a number of problems due to its special geometry and high sensitivity at

very low film thicknesses. The most reliable and easy way of calibrating this probe seemed to be to compare its capacitance value to the 0.635 cm band probe. With the two types of probes mounted close to each other on the test section, capacitance values of both type of probes were recorded simultaneously under the same flow condition. Several test runs were performed to ensure reproducibility of the calibration data. Four third degree curve fits were generated for relation between 0.635 cm band probe and the split-D's ($_{A}D_{1-2}$, $_{A}D_{1-G}$, $_{B}D_{3-4}$ and $_{B}D_{3-G}$)*. Thus, indirect relationship of film thickness with capacitance value can be found through the use of the calibration of the band probe. The results are tabulated in Figure 8 and table 2 in Appendix A.

3.2 Film thickness measurement

Experiments were carried out in two parts, first with free falling film flow, then with counterflow of air. Eight sets of water flow rates ranging from 2.28×10^{-5} m^2/s to 6.17×10^{-4} m^2/s at seven sets of superficial** air velocity (from 0 m/s

*$_{A}D_{1-2}$ represent the electrode pairs between the two 'D' of the split-D probe A while $_{A}D_{1-G}$ represent electrode pairs between one 'D' and the outer ground surface, and same for the $_{B}D_{3-4}$ and $_{B}D_{3-G}$

**Superficial air velocity was based on the entire annular flow cross-section area.

to 7.62 m/s) were chosen as the test matrix. During each run, water flow rate was kept constant and air flow rate was increased up to the condition where the test column started to dry out.

Before wetting the test column, a dry reading was taken for each film probe, which formed the base for every capacitance change. A "very thick film" reference reading was obtained by filling the space between inner and outer tube with stationary water. These two readings were used to normalize the capacitance values. Typical examples are given in table 2 in Appendix A.

All data were recorded on the strip-chart recorder. About two minutes of capacitance response were allowed for each data point to settle and provide a good integrated average value. The 0.635 cm band probe, split-D probes ${}_{A}D_{1-2}$ and ${}_{A}D_{1-G}$ were chosen for the counter flow study, with split-D probes ${}_{B}D_{3-4}$ and ${}_{B}D_{3-G}$ expected to have similar results. All data were checked for reproducibility.

A medium water flow rate was picked for interface profile study where series of pictures for various air flows were taken and fluctuation limits were recorded.

3.3 Flow Measurements

The 'electronic module' was calibrated for both channels on current (I) and resistance (R_p), one channel being designated

for each EP probe. Only six air flows for each water flow rate were used for EP measurement. This is because at highest air flow, probe surfaces dried out and the resistance and current measurements are irrelevant. All other flow situations were carefully matched and checked with the split-D probe. Data for both channels were recorded and integrated by the strip-chart recorder.

3.4 Entrainment Measurement

The drainage flow rate Q_D was determined by collection of draining water at the bottom of the test section over a period of time. The overall entrainment rate can be obtained by subtracting the drainage rate from the liquid feed rate Q_L. This would be an entrainment rate over the entire length of the test section. Six air flows and seven water flow rates were chosen for this study. Two independent runs and several spot checks were carried out during the course of data gathering to ensure reproducibility.

3.5 Data Reduction and Presentation

3.5.1 Film Thickness

Average capacitance readings interms of millivolts were normalized ($\Delta C/\Delta Cm$) and the corresponding film thickness δ was

obtained from the calibration equation. If the capacitance reading was from the split-D probe, another calibration equation (see Table 2 in Appendix A), which related the band probe to the split-D probe, was used to obtain δ. Calibration equation of the 0.635 cm band probe was checked by comparing free film data with laminar theory (this is shown later in Figure 13).

Since the air flow rate was varied for each constant water feed rate in the experiment, data from the 0.635 cm band probe, split-D $_{A}D_{1-2}$ and split-D to ground $_{A}D_{1-G}$ have been plotted as film thickness versus air flow rate with liquid feed rate as parameter (see Figure 9-11, data are also given in tables 3-5 in Appendix A). All calculations, polynomial curve fits and plotting of data were performed using the CDC-6400 computer at Lehigh University.

3.5.2 Entrainment

Averaging from two entrainment runs, final data of drainage flow rate Q_D were obtained and are plotted against air flow rate in Figure 12. Table 6 in Appendix B gives all entrainment data as well as a normalized drainage ratio which will be discussed in the following chapter.

3.5.3 Film Flow

The mean current I and ohmic resistance R_p of the EP probe were converted back to mAmp and k-Ω respectively with the help of the calibration curve of the electronic module.

The effect of air flow rate on I and R_p with liquid feed rate as parameter are shown in Figure 21 to 24 for both channels (data are also given in Table 8 in Appendix C).

3.6 Errors in the Measurement of Film Thickness

Although special care was taken to reduce systematic error by means of calibrating all the measuring instruments, random error is still unavoidable.

Error may arise from the process of calibrating the capacitance probes. The accuracy of the capacitance meter is ±0.005% full scale or ±0.01 pF at 200 pF range. Capacitance signal is integrated by a strip-chart recorder with an uncertainty of ±0.25 mV (±0.025 pF). An error of ±1 mV in reading (visually) the strip-chart value would correspond to an error of 0.1 pF capacitance measurement. Thus the maximum error (ϵ_m) of a capacitance reading would be totally ±0.135 pF.

The error of the calibration equation (see Tables 1 and 2 in Appendix A) is:

$$\epsilon(\delta) = .635 \left\{\frac{2\epsilon_m}{\Delta C_m}\left(1 - \frac{\Delta C}{\Delta C_m}\right)\left[A_1 + 2A_2\left(\frac{\Delta C}{\Delta C_m}\right) + 3A_3\left(\frac{\Delta C}{\Delta C_m}\right)^2\right]\right.$$

$$\left. + \left(\frac{\Delta C}{\Delta C_m}\right)\left[\epsilon A_1 + \epsilon A_2\left(\frac{\Delta C}{\Delta C_m}\right) + \epsilon A_3\left(\frac{\Delta C}{\Delta C_m}\right)^2\right]\right\} \qquad (3.1)$$

where

$\varepsilon(\delta)$ = error in film thickness prediction

$\varepsilon A_{1,2,3}$ = error in coefficient of polynomial calibration curve

ε_m = error from instruments and reading error,

For a typical (3.2×10^{-4} m^2/s) free falling film flow measured by 0.635 cm band probe:

$\Delta C = 7.802$

$\Delta C_m = 67.739$

$\varepsilon A_1 = 0.0207475$; $A_1 = 0.6624046640$

$\varepsilon A_2 = 0.0801569$; $A_2 = -.1823571172$

$\varepsilon A_3 = 0.0745410$; $A_3 = 0.9393654859$.

From Equation (3.1) we have

$$\varepsilon(\delta) = \pm 0.002412 \text{ cm}$$

or

$$\delta = 4.782 \times 10^{-4} \text{ m} \pm 2.412 \times 10^{-5} \text{ m}$$

of about $\pm$ 5% error in film thickness. The worse error in estimating the film thickness is $\pm$ 5.6% at the maximum liquid flow rate, which is small as compared to the total film thickness.

Other sources of error in predicting the film thickness would be in calculation of liquid flow rate and initial calibration of the band probe. Liquid feed rate was read from a rotameter with

an uncertainty of $\pm$ 1% of full scale (1.02×10^{-4} m^3/s), which corresponds to an error of $\pm$ 1.02×10^{-6} m^3/s. At a medium flow rate ($QL = 3.2 \times 10^{-4}$ m^2/s) of zero air flow, the error of film thickness is approximately $\pm$ 1.524×10^{-6} m, which is negligible.

The reading error of the measuring cylinder in the initial calibration of the band probes would be $\pm$ 1 cc of water, which corresponds to an error of $\pm$ 6.218×10^{-6} m in film thickness. Other minor sources of error in film thickness measurement are errors associated with change of capacitance value along the leads and errors due to electrical noise.

4- DISCUSSION OF RESULTS

4.1 Falling Liquid Film

The experimental data without interfacial shear, which covers both viscous and turbulent flow regimes are plotted in Figure 13, where a comparison is made with the Nusselt's laminar film equation as well as with Dukler and Bergelin [3] theory mentioned earlier in Chapter 1. From Figure 13, at a flow rate of approximately 3×10^{-4} m^2/s (Reynolds number of 1165, where roughly transition of laminar to turbulent occur) and below, the experimental data agree closely with the laminar theory. A maximum deviation of the data from the theoretical line is 9% for the band probe and 8% for the split-D probe, which indicate an instrument accuracy better than 1.8×10^{-5} m.

In turbulent region, experimental data starts to deviate from the viscous film equation as expected. Data from the band probe seem to have better agreement with the Dulker and Bergelin theory than does the split-D data, which have a maximum deviation of about 7.2%. It is noted that the band probe has an error band of 3.5% of the average value in the lowest flow rate and 11.3% of the average value at the highest liquid flow rate, while the split-D fluctuated from 4% of the lowest flow rate to 13.4% at the highest flow rate from the average value. Thus, the 7.2% deviation is well within this

fluctuation limit. Blass's [23] experimental results also fall below the Dukler and Bergelin prediction, but with a wider scatter. An average value of the magnitude of fluctuations is shown on the graph for comparison.

As the fluctuation values of the two probes indicates, the split-D probe appears to be more sensitive than the band probe. The reason may be due to two factors. First, the split-D measures local instantaneous film thickness while the band probe measures the integrated value around the flow periphery. Secondly, the gap size between the split-D probe is smaller than the band probe. Since capacitance is inversely proportional to the gap between electrodes (examples found in Figure 8 and 7 - the calibration curves for split-D and band probes), with a steeper change of $\Delta C/\Delta C_m$ with smaller space between electrodes, the split-D probe is more sensitive to change of film thickness. As a whole, both band and split-D probes predict the same thickness of the liquid film when the film is free falling with no interfacial shear, a condition where local fluctuations in film thickness would be small.

4.2 Interfacial Analysis

The effect of air flow on the liquid film is important in understanding interfacial behavior. A set of simple equations

are derived here for predicting film thickness in presence of interfacial shear. Assuming that wall curvature can be neglected, ignoring waves and mass transfer between film and air, conservation of momentum gives;

for laminar flow:

$$\frac{\partial P}{\partial z} + \mu_L \frac{\partial^2 u}{\partial y^2} + \rho_L g = 0 \tag{4.1}$$

assuming $\rho_L g >> \frac{\partial P}{\partial z}$, integration gives

$$-\mu_L \frac{\partial u}{\partial y} = \tau_i - \rho_L g(\delta - y). \tag{4.2}$$

The boundary condition $\tau=\tau_i$ at $y=\delta$ was used to eliminate the integration constant. Again, integration with boundary condition $u=0$ at $y=0$ will give the velocity profile in the liquid film as

$$u = \frac{\rho_L g}{\mu_L} (\delta y - \frac{y^2}{2}) - \frac{\tau_i y}{\mu_L} \tag{4.3}$$

and mass flow rate

$$\omega_L = \int_0^\delta \rho_L u dy \; L \tag{4.4}$$

$$\frac{\omega_L}{L} = \rho_L (\rho_L \frac{g\delta^3}{3\mu_L} - \frac{\tau_i \delta^2}{2\mu_L}) \tag{4.5}$$

and peripheral liquid flow rate is

$$Q_L = \rho_L \frac{g\delta^3}{3\mu_L} - \frac{\tau_i \delta^2}{2\mu_L} \tag{4.6}$$

with $\tau_i = 0$, equation (4.5) reduces to Nusselt equation (1.1). Knowing interfacial shear stress and liquid flow rate, film thickness can be predicted from equation (4.6).

The effect of air flow on film thickness can be seen from Figures 9 to 11. Just before flooding occurs, it was observed that very little change of film thickness took place. There is a small thickening of the film detected by the band probe and one of the split-D probes immediately prior to flooding in the high film flow region. Hewitt and Wallis [13] have speculated that there should have a small increase in thickness from their theoretical prediction of film thickness before flooding, but it was not evident from their own data.

The effect of film flow rate on film thickness is shown in Figure 14. Three air flows below the flooding rate, including the zero air flow rate, were chosen to study the interfacial behavior of the falling film. Notice that the local instantaneous film flow rate cannot be measured from the experiment, because local entrainment rates are not known. Hence, in Figure 14, an approximate local film flow rate is used (based on linear entrainment between inlet and outlet - discussion

in the next section). The three constant air flow curves in Figure 14 seem to merge together at the lower film flow region, indicating that air flow has less effect on thinner films even at high air flow rates. At higher liquid flow rates, there is a more pronounced effect, but the maximum increase in thickness is only about 3.1% from the case of zero air flow.

Figure 15 shows the relation between interfacial shear stress and air flow rate. The interfacial shear τ_i was obtained from equation (4.6), with film flow rate and film thickness data as input parameters. In this calculation, physical properties of air and water were taken to be: liquid density (ρ_ℓ) = 997.4 Kg/m^3; liquid viscosity (μ_ℓ) = 9.8 x 10^{-3} kg/ms and air density (ρ_g) = 1.205 kg/m^3. The negative value of τ_i appearing on the graph may be due to film thickness data which fall below the theoretical free film curve for the lowest liquid flow case. With the exception, interfacial shear was found to increase with increase in air flow as expected physically. A correlation of shear stress with air flow is not possible at this stage due to insufficient usuable data before the flooding point.

A cross plot of Figure 15, and Figure 16 relates shear stress to film flow rate at constant air flow, a steeper change

of shear stress with film flow is seen, probably associated with the wavy and rough surfaces at the higher film flow rate. As compared with Figure 15, air flow rates seem to have less effect on interfacial shear stress than liquid film flow rate, which may explain why film thickness does not vary much as air rate increases up to flooding.

Figure 17 shows the relationship between film thickness and film flow rate with interfacial shear stress as a parameter (Equation 4.6). Dukler [8] also showed a similar figure but with cocurrent downward flow, his parametric curves lie below the theoretical free film curve while the present countercurrent study lie above the viscous free film line as expected. Also shown in Figure 17 are data of the 0.635 cm band probe before flooding. The data falls within a narrow range of interfacial shear stress (0-1.2 N/m^2) which confirm the behavior of film thickness (as shown previously in Figures 9-11) before the flooding point is reached.

Typical expanded wave profiles representing different air flows at a constant liquid feed rate are given in Figure 18. These are the output signals of the capacitance probe as seen on an oscilloscope. Approximate amplitudes of the surface waves can be determined from the scale along the side of each photographic trace. A comparison of Figure 18(a) and (b)

indicates that the character of the interfacial wave does not change much in the air velocity range of 0-3.1 m/s except for a slight increase in frequency. However, at higher air flows (c) and (d), a marked increase in amplitude and frequency is observed, which would correspond to onset of flooding. Beyond the flooding point, wave frequency decreases and a sharp decrease in the mean film thickness can be seen (similar to that observed in Figure 9-11).

4.3 Entrainment and Flooding

4.3.1 Entrainment

The disturbance waves in countercurrent flow are usually regarded as being the sources of liquid entrainment, which starts with roll off of liquid from the film surface into the gas stream. The onset of entrainment in the present experiment can be detected by noticing droplets striking the unwetted outer wall, but the main concern here is to estimate the actual film flow rate. Since the local film flow could not be measured, a rough linear relationship of the inlet and drainage liquid flowrate with position of the test probe is assumed.

$$Q_F = Q_L \left(\frac{\ell_o - \ell}{\ell}\right) + Q_D \left(\frac{\ell}{\ell_o}\right) \qquad (4.7)$$

This relationship satisfied the inlet condition at $\ell=0$ and outlet condition at $\ell=\ell_o$, where ℓ is the position of the test probe relative to water inlet and ℓ_o is the total length of the test rig. Experimental observation showed liquid droplets being torn off the film surface even at location close to the air entrance, consistant with the above equation.

The drainage data obtained were normalized with liquid feed rate and plotted against gas velocity in Figure 19. From the graph it was found that higher liquid feed rates are more subject to entrainment at lower air velocities, which is consistent with increase interfacial shear in higher film flow. The figure also shows the onset of flooding, characterized by a sharp increase in entrainment (decrease in drainage).

4.3.2 Flooding

The onset of flooding may be detected from the film thickness data of Figure 9-11 or from the entrainment data. The gas rates and liquid rates at which the onset of flooding took place, as read from each of these figures, are plotted in Figure 20 in terms of dimensionless superficial velocities:

$$Vg^* = Vg\rho_g^{\frac{1}{2}}[gD(\rho_\ell-\rho g)]^{-\frac{1}{2}} \qquad (4.8)$$

and

$$V_\ell^* = V_\ell \rho_\ell^{\frac{1}{2}} [gD(\rho_\ell - \rho_g)]^{-\frac{1}{2}} \quad . \tag{4.9}$$

The numbers shown above each data point in Figure 20 represent the number of times that particular data point was reproduced by a particular instrument. Table 7 in Appendix B lists the observed gas and liquid velocities at the flooding point.

A general Wallis Correlation [19] with

$$\sqrt{V_g^*} + m\sqrt{V_\ell^*} = C$$

where m=1 for turbulent flow and C varies depending on the entrance and exit geometries. Regression analysis of the present data gives m=0.78 and C=0.50, and the average deviation of data from the above expression is 2.73%. The value of C is quite different from those observed in experiments of flooding inside tubes (reported values of C range from 0.725 to 1.0 for tube flow). Presumably this is because of different entry and exit conditions and the nature of the annular film flow (outside the rod surface in the present case). No general validity for these coefficients can be claimed because of small data base.

4.4 Flow Measurement

As stated earlier, the EP (electrolysis potential) probe was used to measure liquid flow rate. Figure 21 to 24 show

typical current and ohmic resistance behavior of the EP probe at 100 volts applied dc potential across the electrodes of the two EP probes (1 and 2). Data from each probe show that current increases with liquid flow and decreases with film thickness, whereas ohmic resistance decrease with increase liquid flow and increase with decreasing film thickness.

Film thickness effects become noticeable at higher air flow (on and beyond flooding) at which the film velocity becomes irrelevant. The thinning of the liquid film due to heavy entrainment increases the air to surface contact, resulting in increase of ohmic resistance and decrease of current.

The output signals of the EP probe (I and R_p) are dependent, among other things, on the film thickness. Since the film is wavy in nature, these signals would show a fluctuating behavior.

In the tests conducted, it was found that R_p fluctuated by 6% to 32% as the liquid flow rate increased from the minimum to the maximum value. The current varied by 8% to 16% about the mean over the same range of liquid flow rates. However, for each test, it was possible to obtain an integrated average value of I and R_p for a particular liquid feed rate, gas flow rate and average film thickness.

Figure 25 shows the effect of flow rate on the product (IxR_p) of EP probe #2 (EP probe #1 would be similar). Also

shown in Figure 25 is the mean film thickness detected by the split-D probe at the same gas and liquid flow rates. The behavior of the product (IxR_p) is similar to those observed in earlier tests in bounded films and films with no interfacial shear [22]. This indicates that the EP probe is indeed capable of operating meaningfully in a counter-current flow situation. Further tests, with more detailed measurements over a wide range of gas and liquid flow rates should be carried out to obtain 'calibration' data. Such a detailed calibration procedure was considered outside the scope of the present investigation. The present data on I and R_p have been tabulated in Appendix C.

5- SUMMARY AND CONCLUSIONS

1) Film thicknesses on the outside surface of a cylindrical rod have been measured for water films in downward flow in the presence of counterflow air. The measurement was carried out using newly developed capacitance probes [21,22] of two different geometries.

2) At zero air flow rate, the measured film thicknesses compare very well to available laminar and turbulent film theory for free films, attesting to credibility of the measurement technique.

3) Before the onset of flooding, there was very little change in film thickness as air flow rate was increased at a constant water feed rate. This is in conformity with previous observations on counter-current annular flow [19] on the inside of vertical tubes.

4) The interfacial shear stress, calculated from the data by a simple force balance using laminar theory, was found to be strongly dependent on liquid flow rate and very weakly on the gas flow rate. Typical values of the interfacial shear stress were in the range 1-1.2 N/m^2.

5) Air-water flooding data have been obtained in an annular geometry, and can be represented with the Wallis Correlation [19].

6) The fast response of the capacitance probes used for film thickness measurement allowed continuous tracking of the liquid film surface up to and beyond the flooding point. Thus, it was possible to obtain a description of the film surface with increasing interfacial shear rates. The results show that before flooding, the mean film thickness is insensitive while the wave frequency is sensitive to interfacial shear.

7) A newly developed concept for film velocity measurement, the Electrolysis Potential Probe [21], was tested in films with interfacial shear. The limited data obtained show that the probe can be calibrated for counter-current flow situations, but further testing is necessary.

BIBLIOGRAPHY

1. C.G. Kirkbride, "Heat Transfer by Condensing Vapor on Vertical Tubes", Industrial and Engineering Chemistry, Vol. 26, No. 4, 425-428, 1934.

2. M.L. Jackson, "Liquid Films in Viscous Flow", A.I.Ch.E. Journal, Vol. 1, No. 2, 231-240, 1955.

3. A.E. Dukler and O.P. Begelin, "Characteristics of Flow in Falling Liquid Films", Chemical Engineering Progress, Vol. 48, No. 11, 557-563, 1952.

4. T. Von Karman, "The Analogy Between Fluid Friction and Heat Transfer", Trans. ASME, Vol. 61, 705-711, 1939.

5. S. Portalski, "Studies of Falling Liquid Film Flow - Film Thickness on a Smooth Vertical Plate", Chemical Engineering Science, Vol. 18, 787-804, 1963.

6. G.H. Anderson and B.G. Mantzouranis, "Two-phase (Gas-Liquid) Flow Phenomena - I", Chemical Engineering Science, Vol. 12, 109-126, 1960.

7. J.G. Collier and G.F. Hewitt, "Date on the Vertical Flow of Air-Water Mixtures in the Annular and Dispersed Flow Regions. Part II: Film Thickness and Entrainment Data and Analysis of Pressure Drop Measurements", Trans. Instn. Chem. Engrs., Vol. 39, 127-136, 1961.

8. A.E. Dukler, "Fluid Mechanics and Heat Transfer in Vertical Falling-Film Systems", Chemical Engineering Progress Symposium Series Vol. 56, No. 30, 1-10, 1960.

9. D.A. Charvonia, "An Experimental Investigation of the Mean Liquid Film Thickness and the Characteristics of the Interfacial Surface in Annular, Two-Phase Flow", ASME Paper #61-WA-243, 1-13, 1961.

10. P.G. Kosky, "Thin Liquid Films Under Simultaneous Shear and Gravity Forces", Int. J. Heat Mass Transfer, Vol. 14, 1220-1223, 1971.

11. E.J. Davis, "An Analysis of Liquid Film Flow", Chemical Engineering Science, Vol. 20, 265-272, 1965.

12. W.M. Rohsenow, J.H. Webber, and A.T. Ling, "Effect of Vapor Velocity on Laminar and Turbulent-Film Condensation", Trans. of ASME, Vol. 78, 1637-1643, 1956.

13. G.F. Hewitt and G.B. Wallis, "Flooding and Associated Phenomena in Falling Film Flow in a Vertical Tube", Multi-Phase Flow Symposium, WAM of ASME, 62-74, 1963.

14. A.E. Dukler and L. Smith, "Two-Phase Interactions in Countercurrent Flow Studies of the Flooding Mechanism", Progress Report, prepared for USNRC, NUREG-0214, June 1977.

15. G.F. Hewitt, P.M.C. Lacey and B. Nicholls, "Transitions in Film Flow in a Vertical Tube", Symposium on Two-Phase Flow", Exeter, 21-23, Vol. 2, 1965.

16. G.B. Wallis, "Flooding Velocities for Air and Water in Vertical Tubes", AEEW-R123, 1961.

17. C.L. Tien, K.S. Chung and C.P. Liu, "Flooding in Two-Phase Counter Current Flows", EPRI, Topical Report, NP-1283, 1979.

18. G.F. Hewitt and N.S. Hall Taylor, "Annular Two-Phase Flow", Pergamon Press, 68-73, 1970.

19. G.B. Wallis, "One-dimensional Two-phase Flow", McGraw-Hill, 330-343, 1976.

20. E. Blass, "Gas/film Flow in Tubes", Internal Chemical Engineering, Vol. 19, No. 2, 183-195, 1979.

21. R.K. Sundaram, E.J. London and J.C. Chen, "Development of Instrumentation for the Measurement of Thickness and Velocities of Thin Water Films", Presented at the Sixth Reactor Safety Research Information Meeting, USNRC, Washington, DC, Nov. 1978.

22. R.K. Sundaram, J.C. Chen, E.J. London and A.T. Fei, "Instrumentation for Film Dynamics in Two-Phase Flow", Presented at 7th Reactor Safety Research Information Meeting, USNRC, Washington, DC, Nov. 1979.

23. G.F. Hewitt, "Measurement of Two-Phase Flow Parameters", Academic Press, 110-180, 1978.

24. Y.Y. Hsu and R.W. Graham, "Transport Processes in Boiling and Two-Phase Systems", McGraw Hill, 369-398, 1976.

25. H.N. McManus, Jr., "Experimental Methods in Two-Phase Flow", Multi-Phase Flow Symposium, WAM of ASME, Nov. 17-22, 1963.

26. S.R. Tailby and S. Portalski, "The Hydrodynamics of Liquid Films Flowing on a Vertical Surface", Trans. Instn. Chem. Engrs., Vol. 38, 324-330, 1960.

27. M.R. Ozgu and J.C. Chen, "A Capacitance Method for Measurement of Film Thickness in Two-Phase Flow", Rev. Sci. Instrum., Vol. 44, No. 12, 1714-1716, 1973.

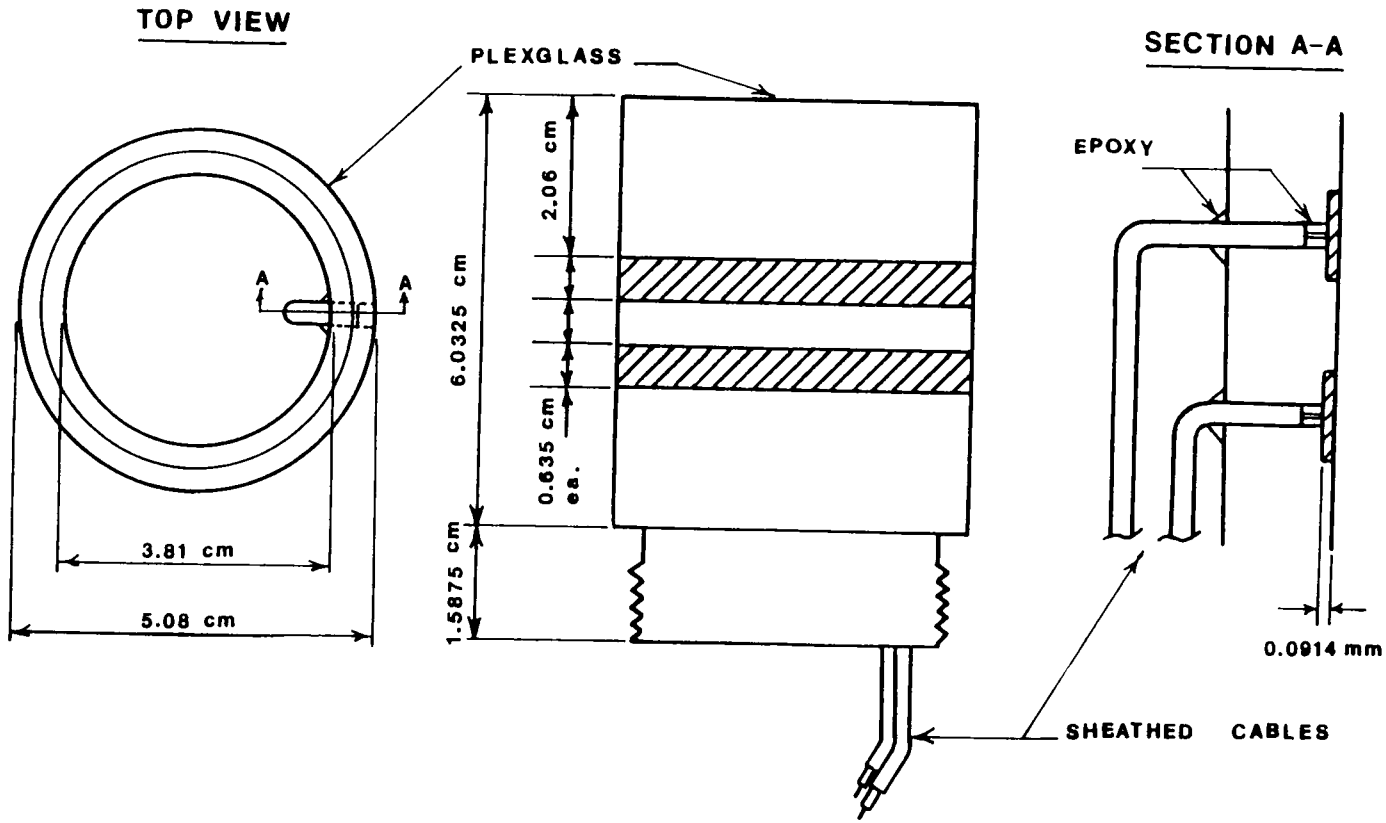

Figure 1. Liquid film measuring device - Band Probe

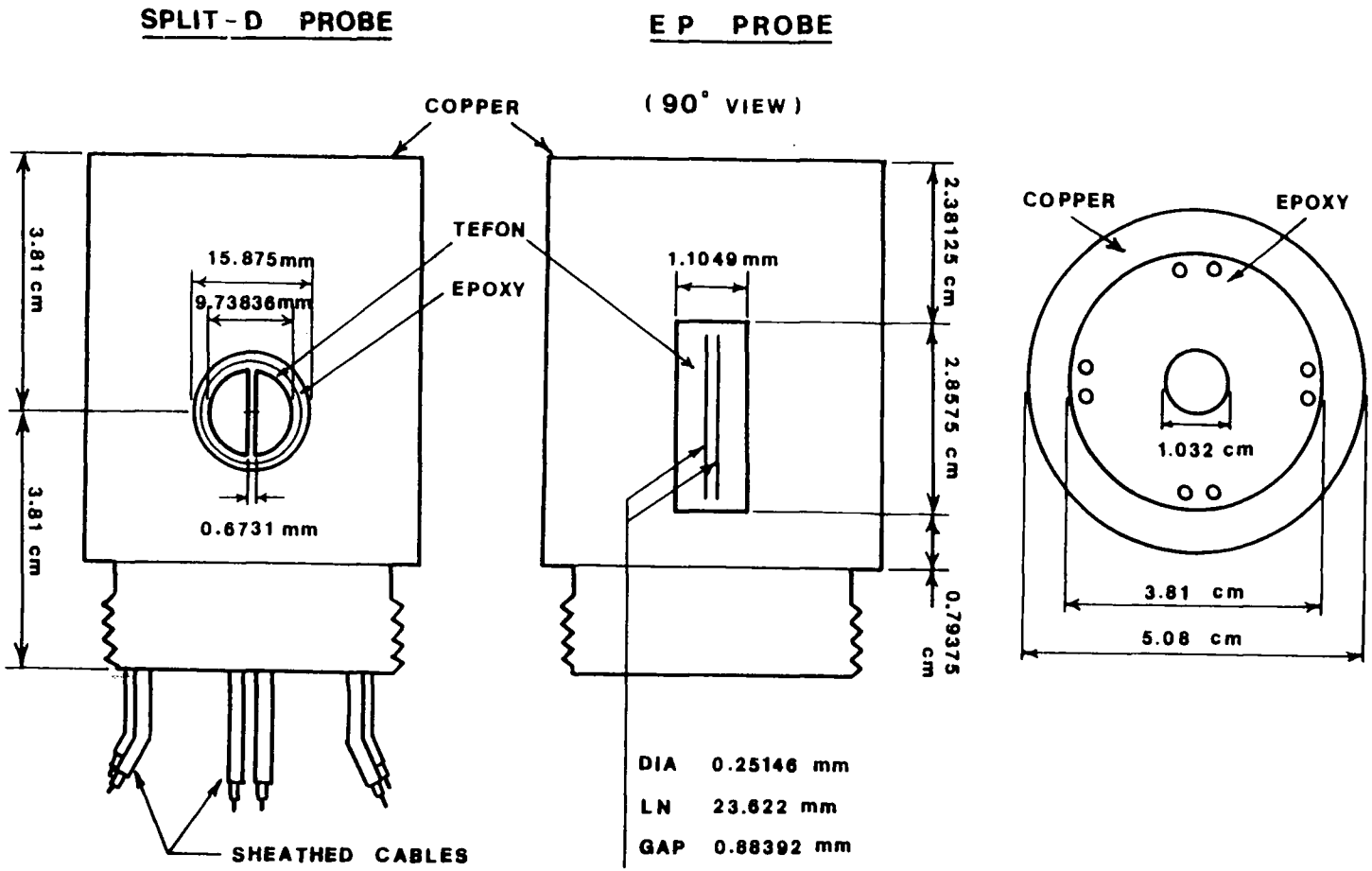

Figure 2. Liquid film measuring device - Split-D & EP Probes

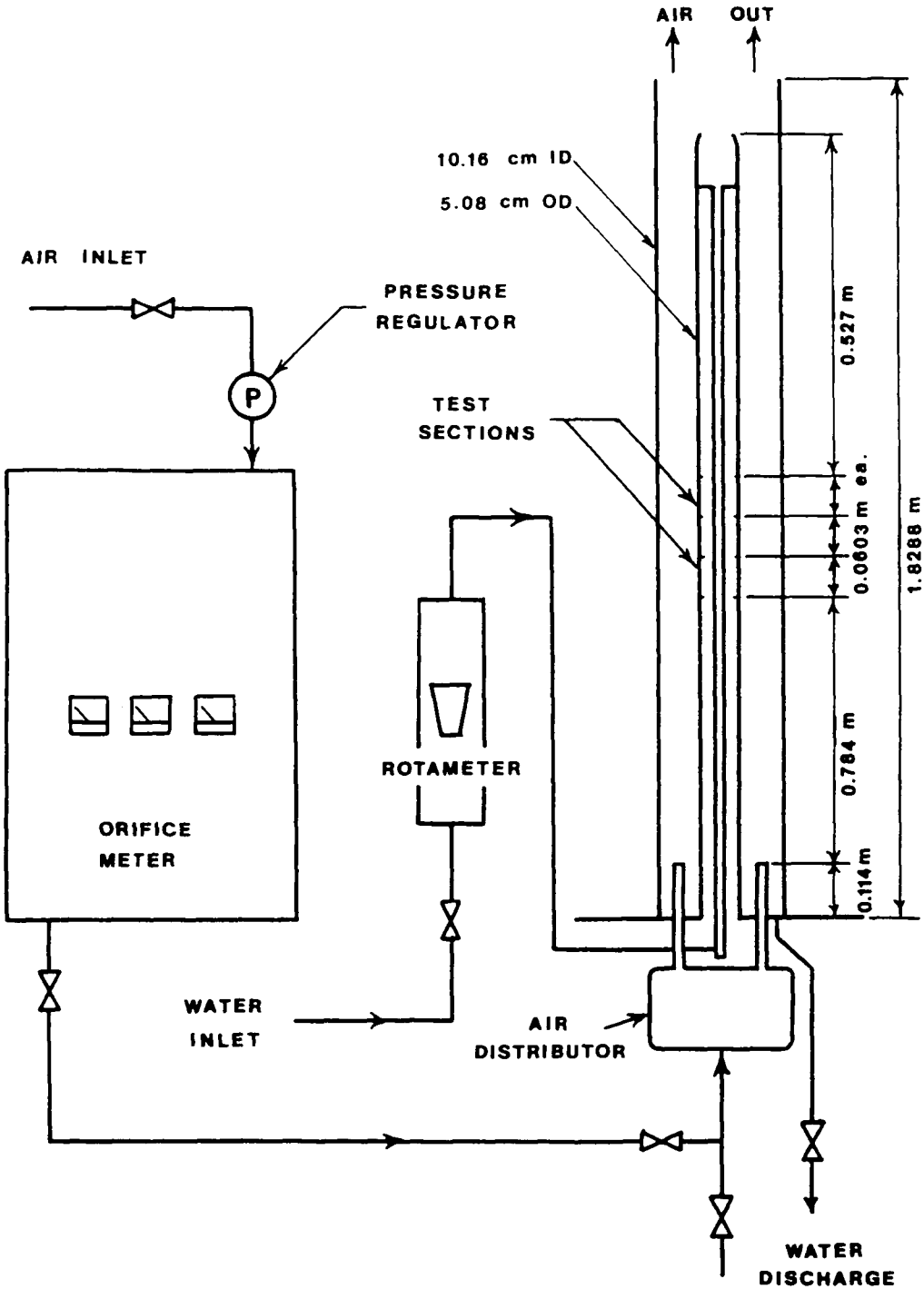

Figure 3. Counter-Current Air-Water rig schematic diagram

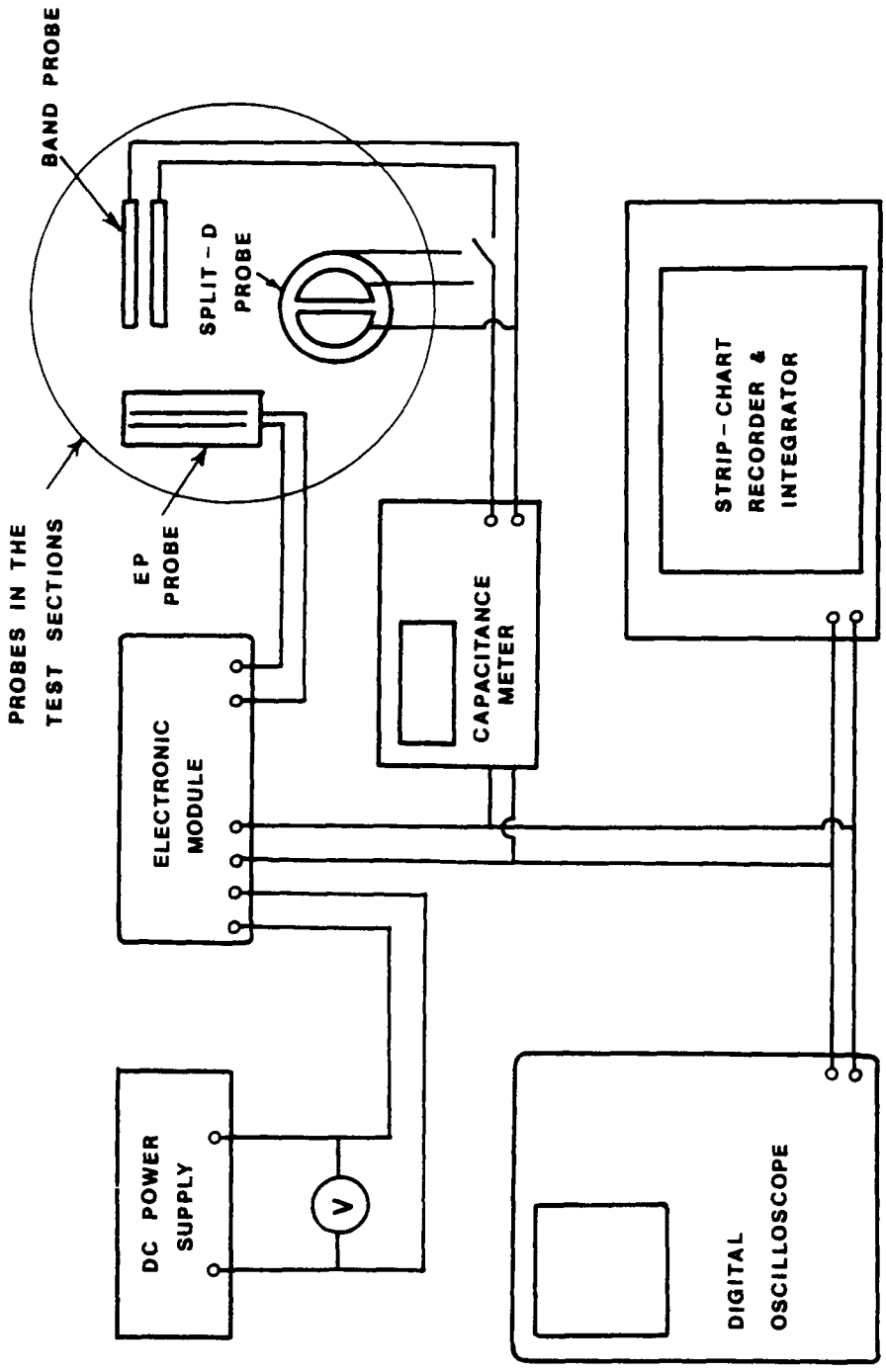

Figure 4. Instrumentation schematic diagram

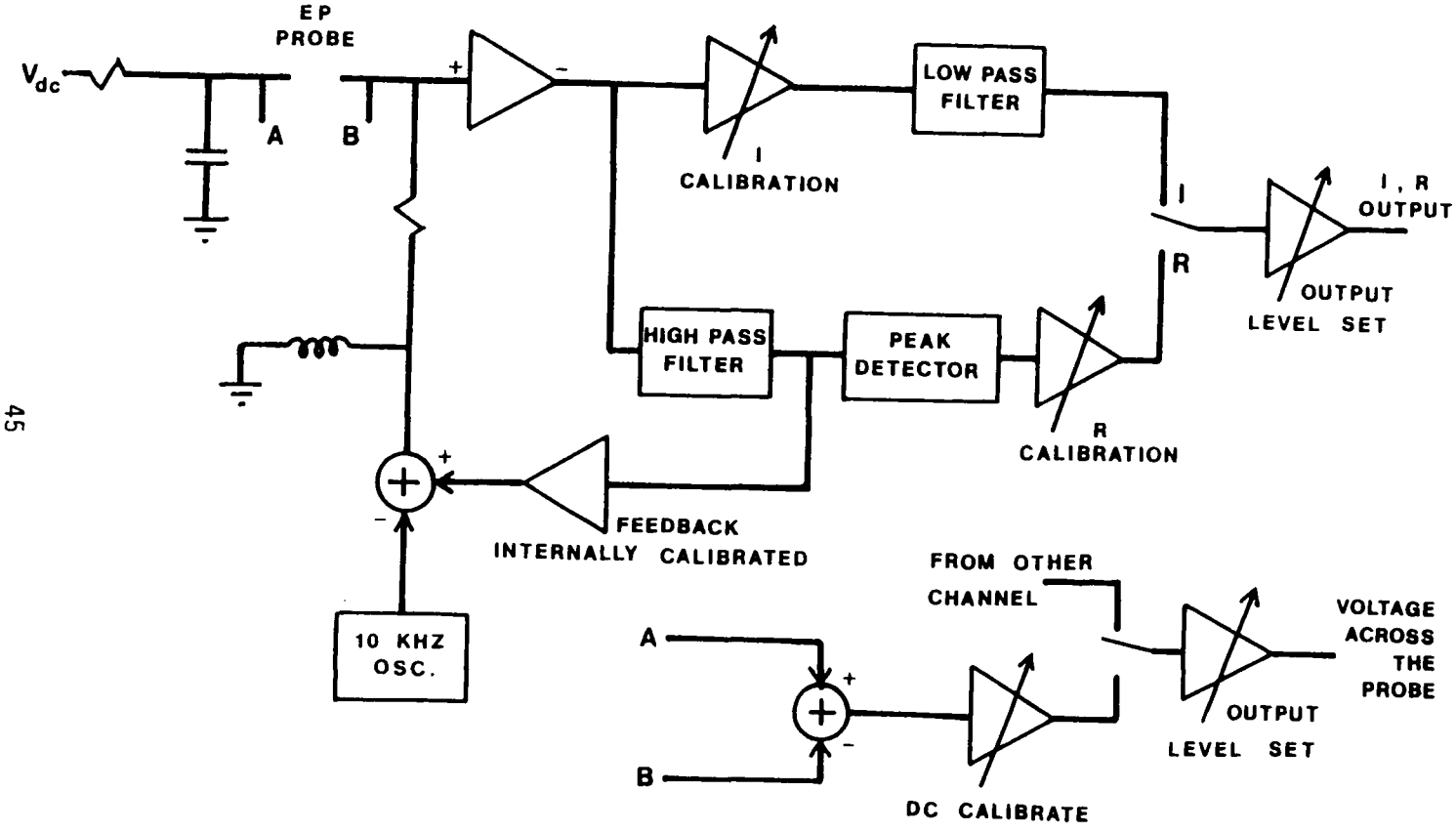

Figure 5. Electronic module circuit diagram

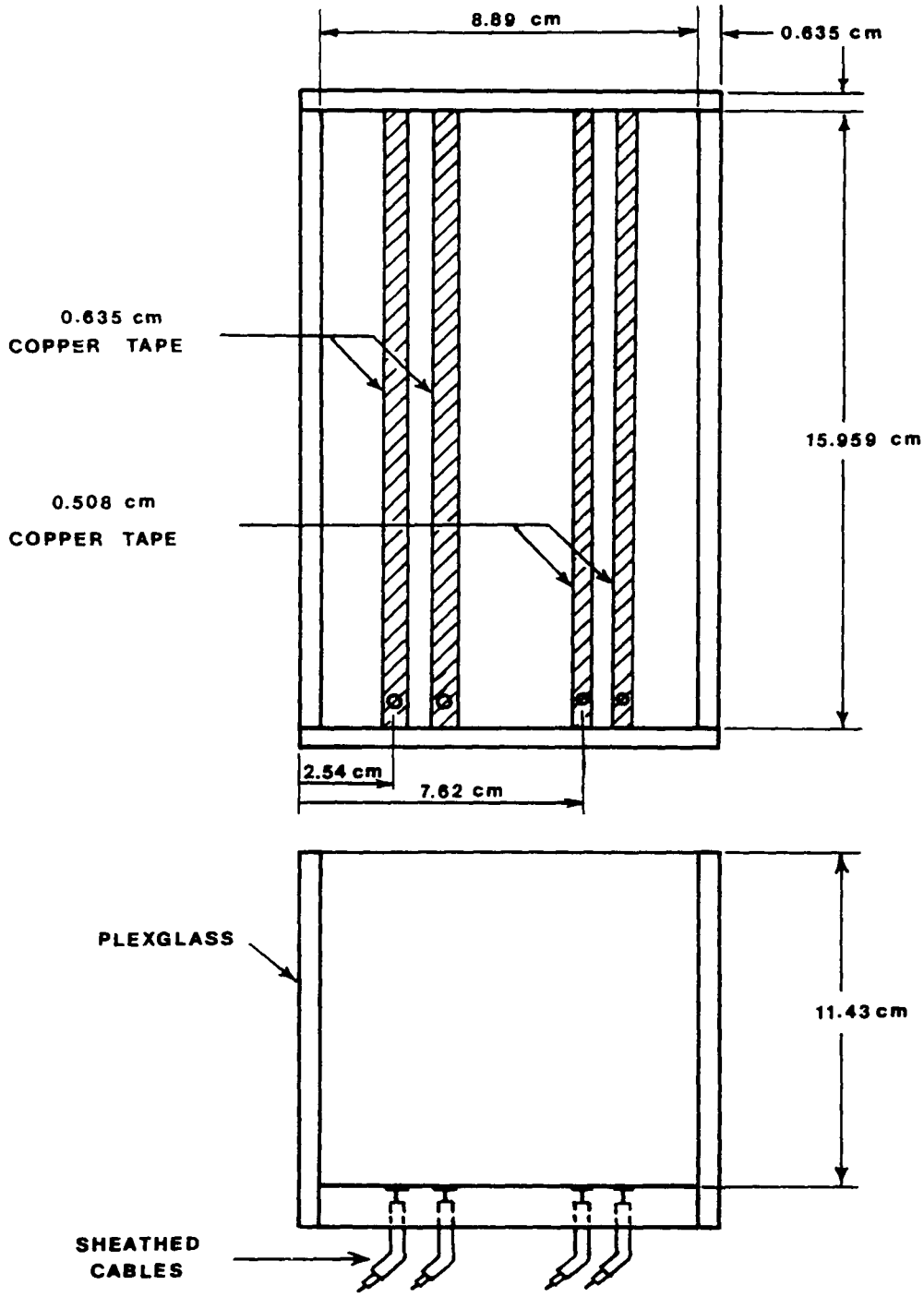

Figure 6. Band Probes calibration device

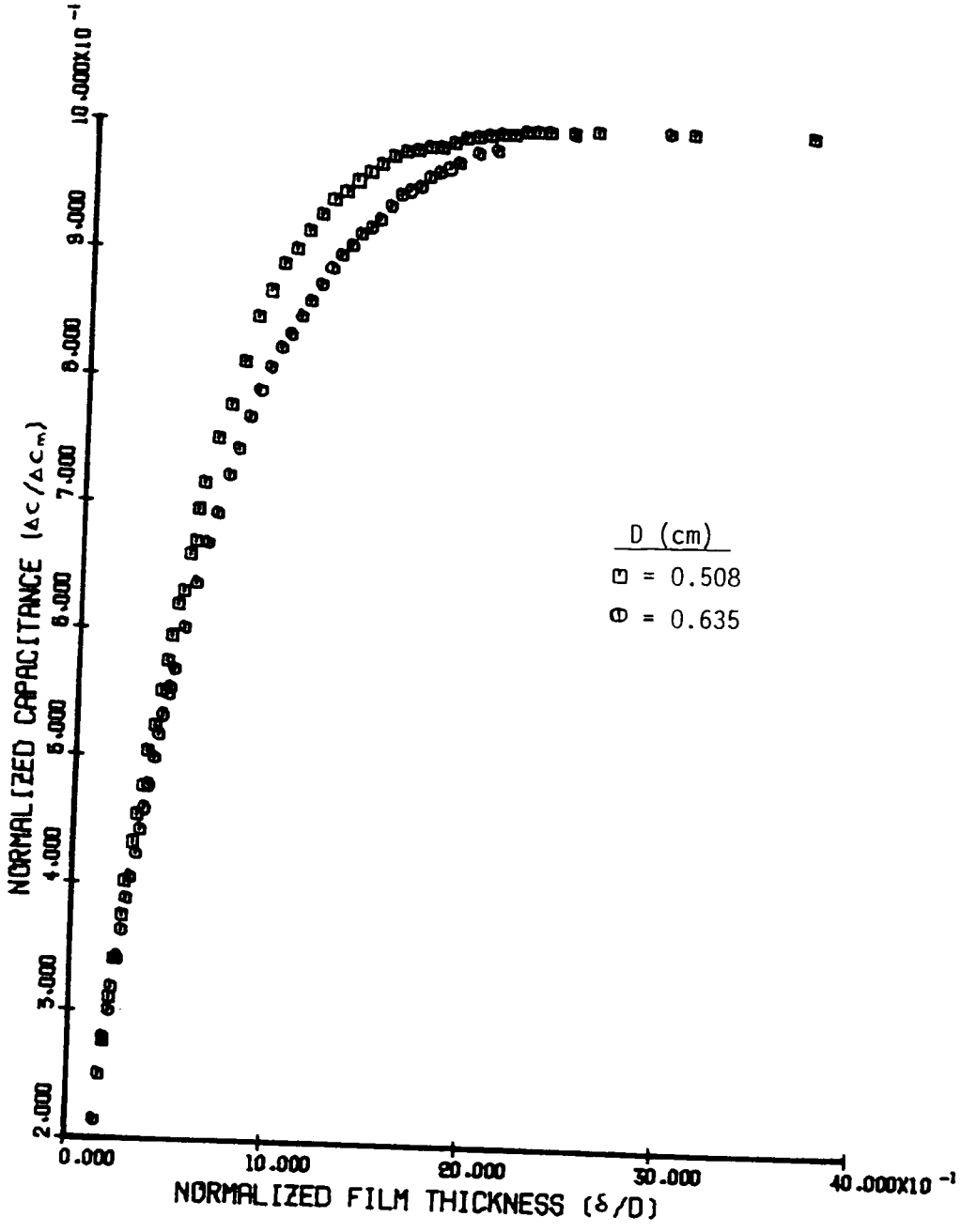

Figure 7. Band Probes calibration

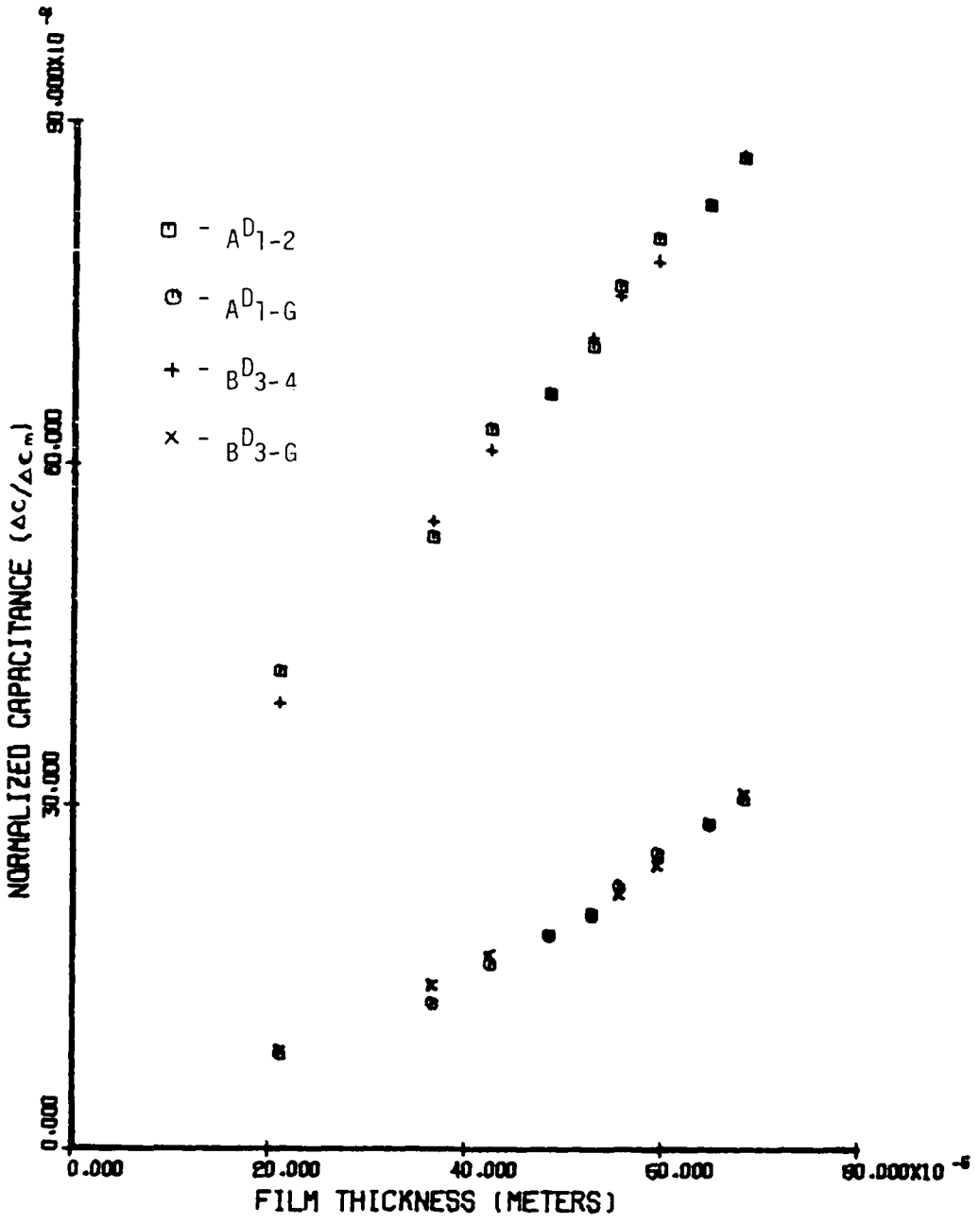

Figure 8. Split-D Probes calibration

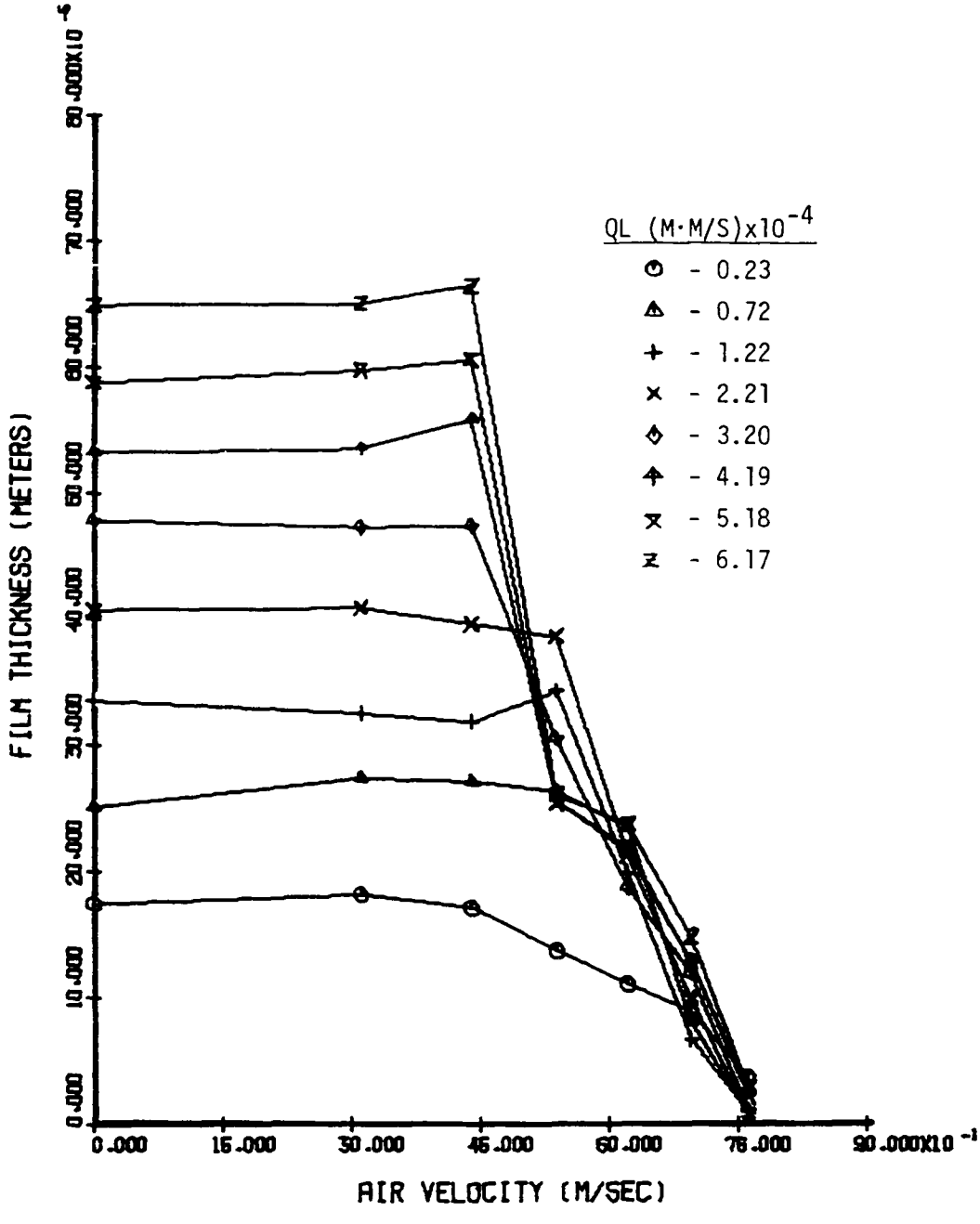

Figure 9. Film thickness at various liquid feed rates - 0.635 cm Band Probe

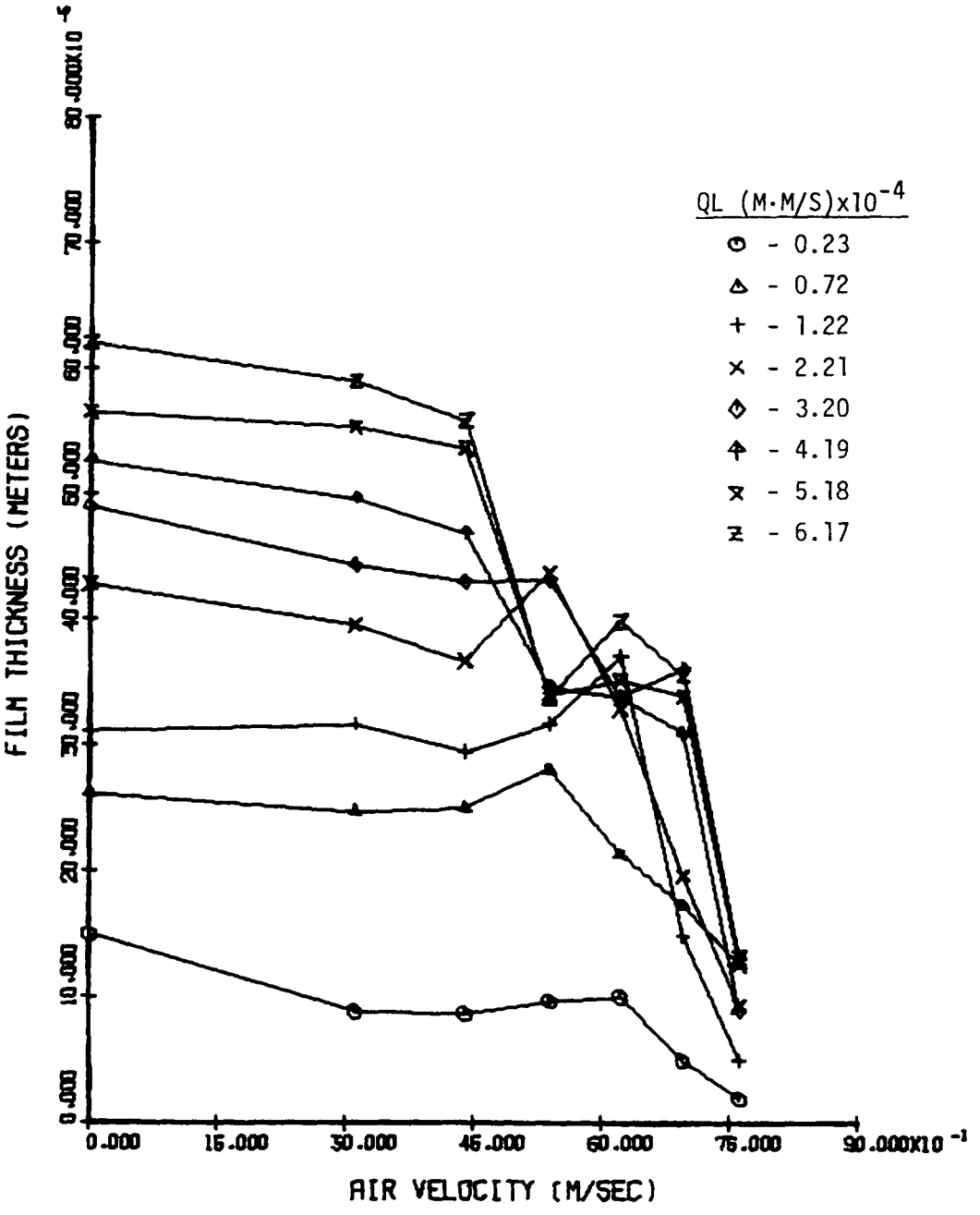

Figure 10. Film thickness at various liquid feed rates - A^{D}_{1-2}

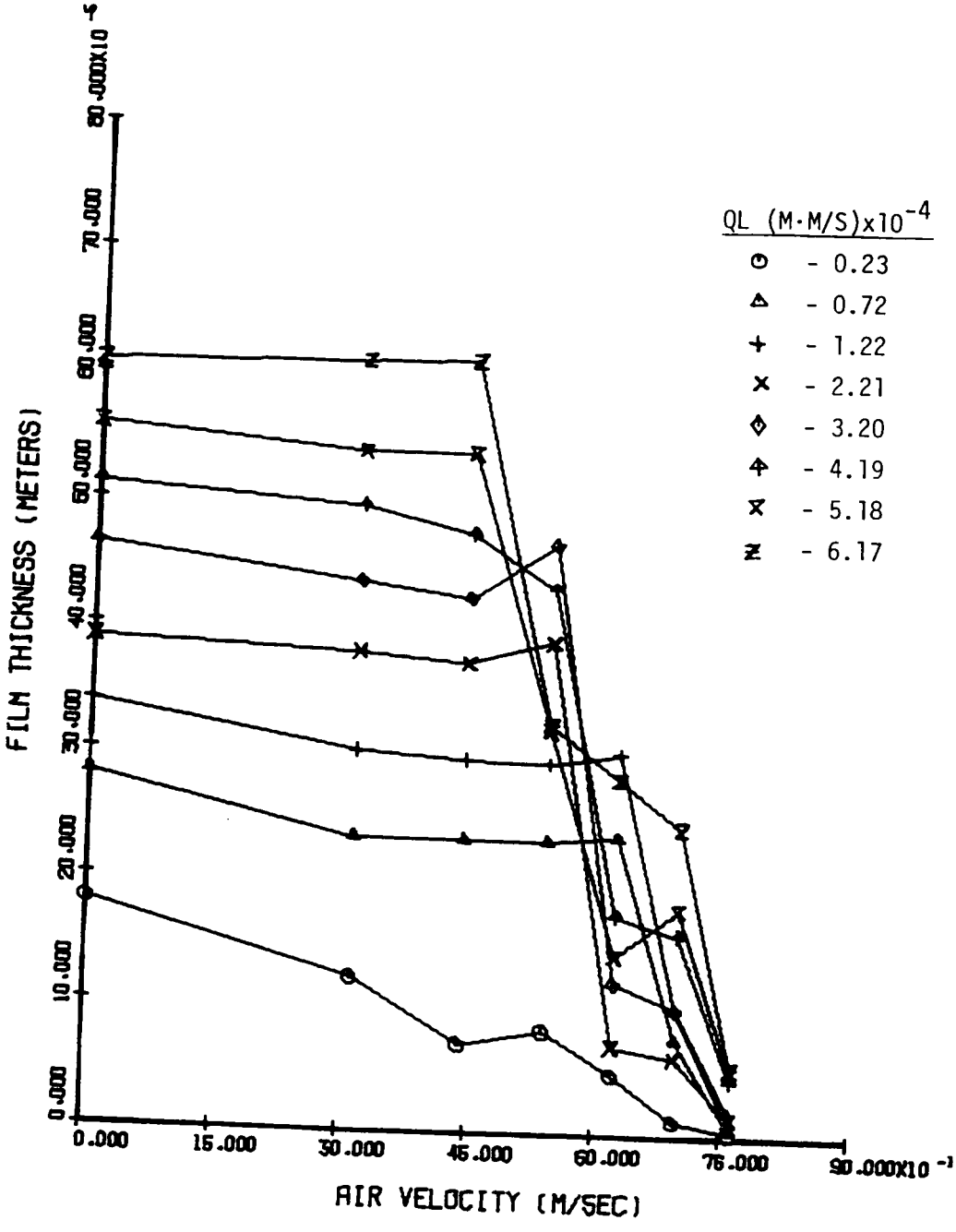

Figure 11. Film thickness at various liquid feed rates - A^{D}_{1-G}

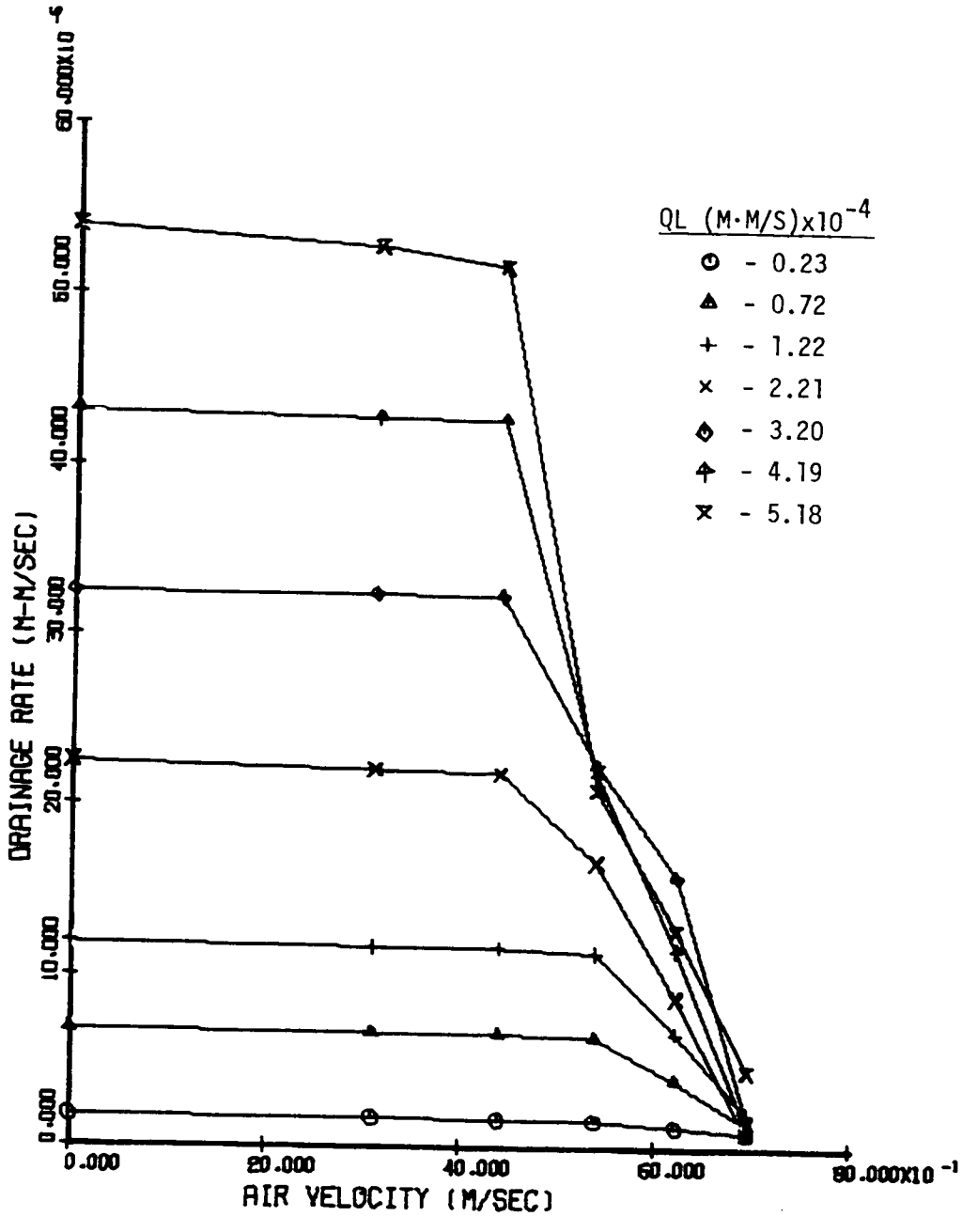

Figure 12. Drainage flow rate at various liquid feed rates

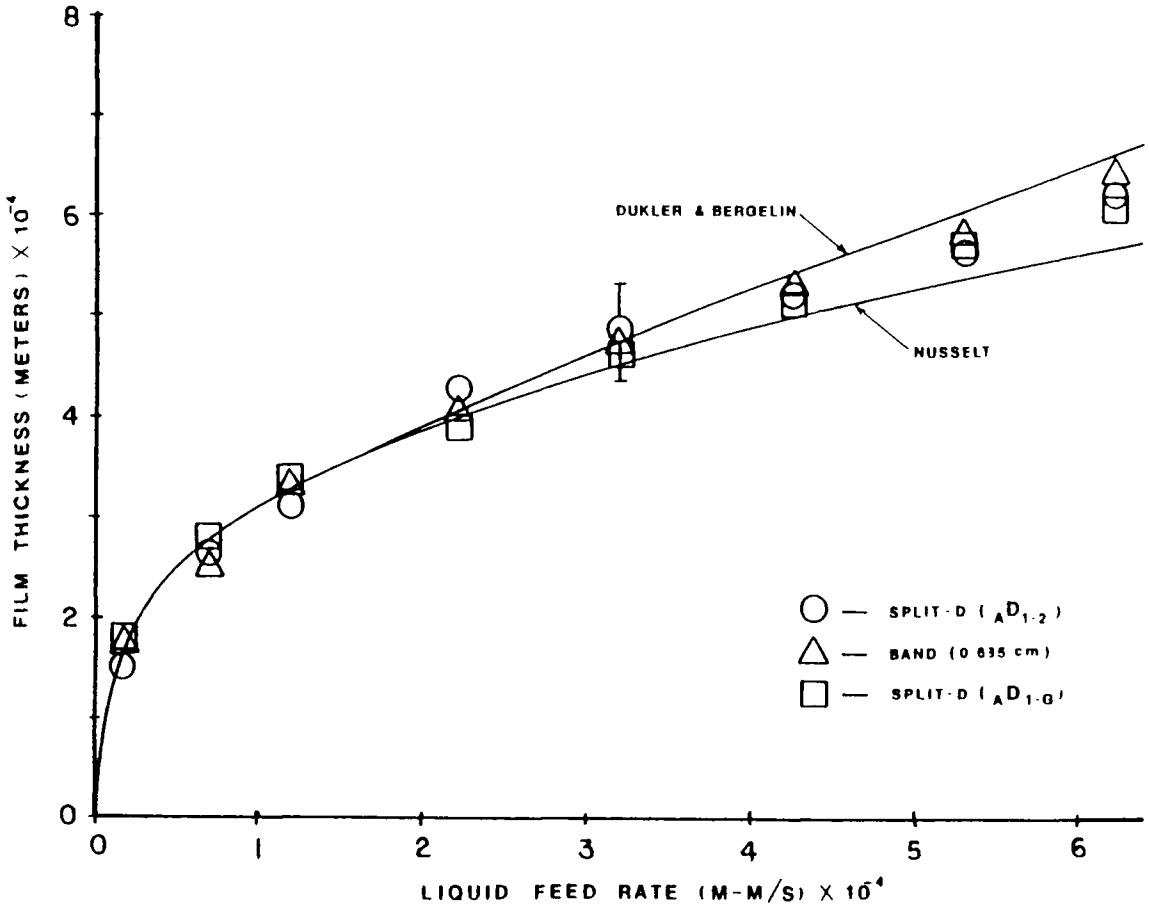

Figure 13. Effect of liquid feed rate on falling film thickness with zero shear at the liquid interface

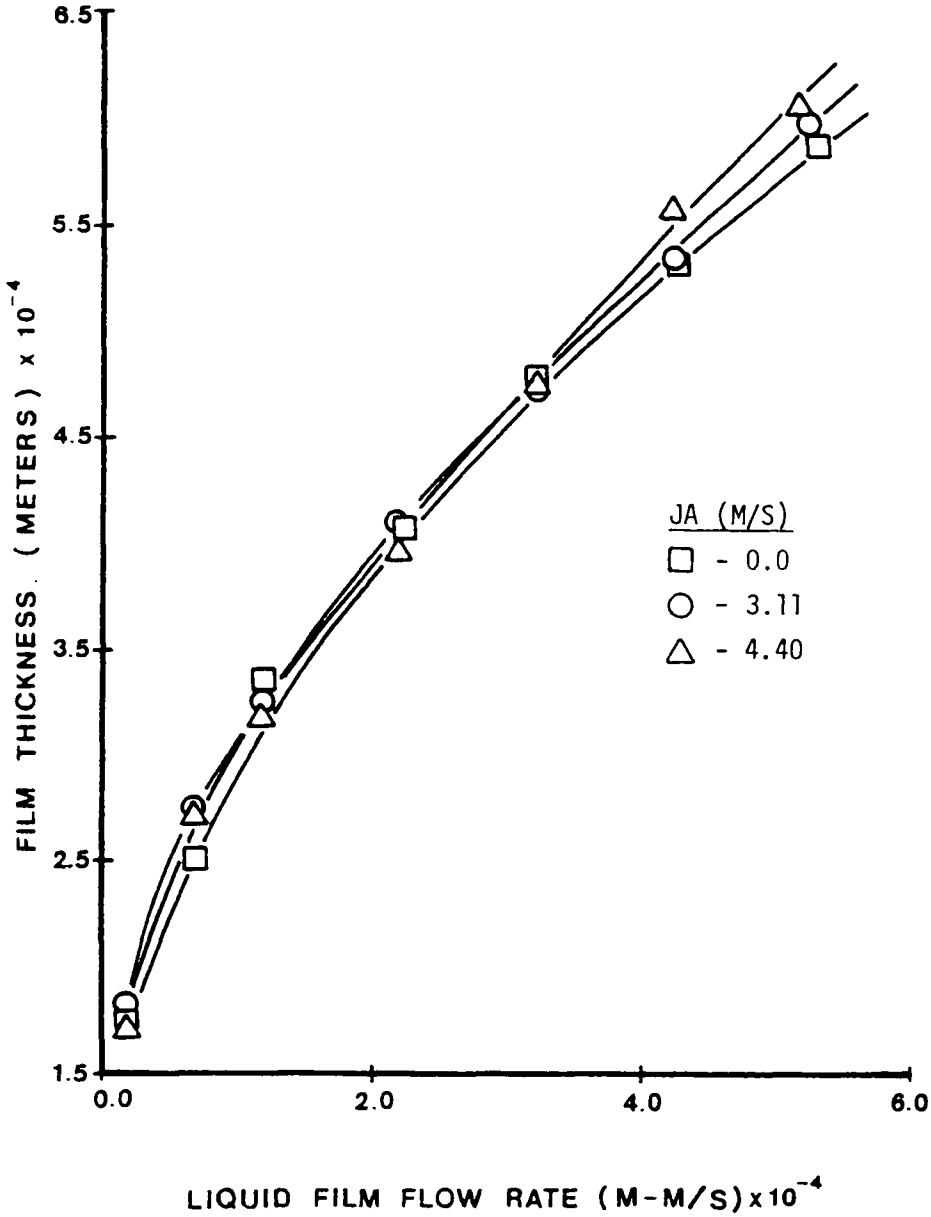

Figure 14. Film thickness at various air-flow rates before flooding

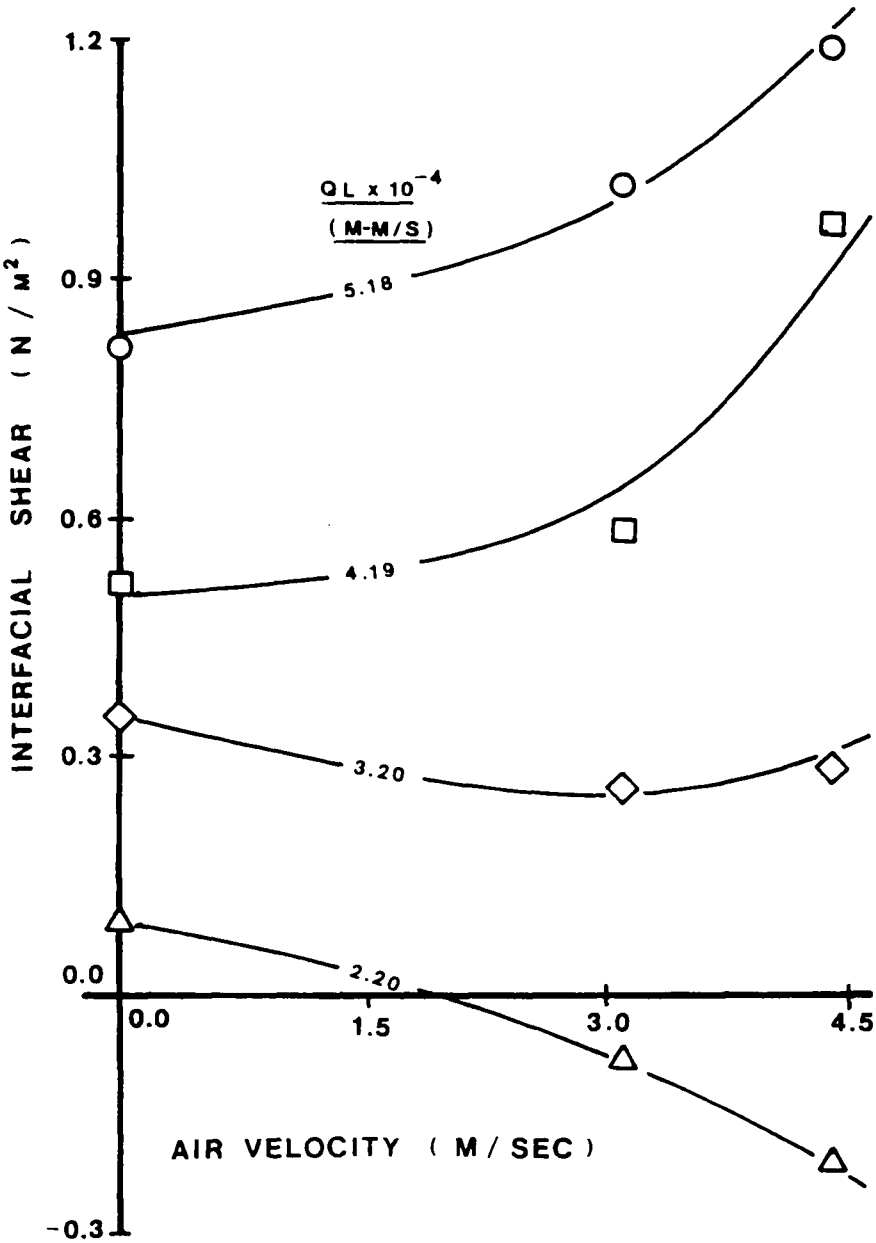

Figure 15. Effect of film flow rates on interfacial shear

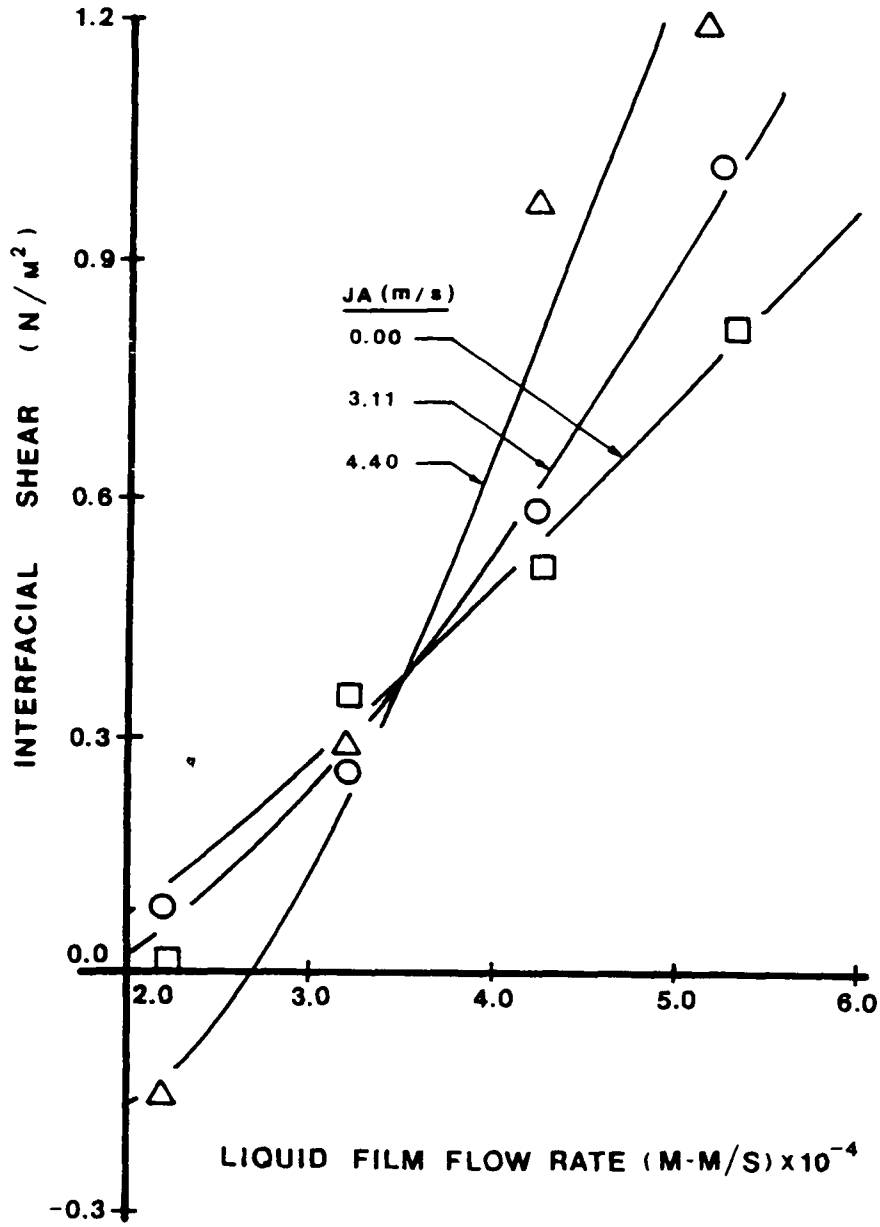

Figure 16. Effect of air flow rates on interfacial shear

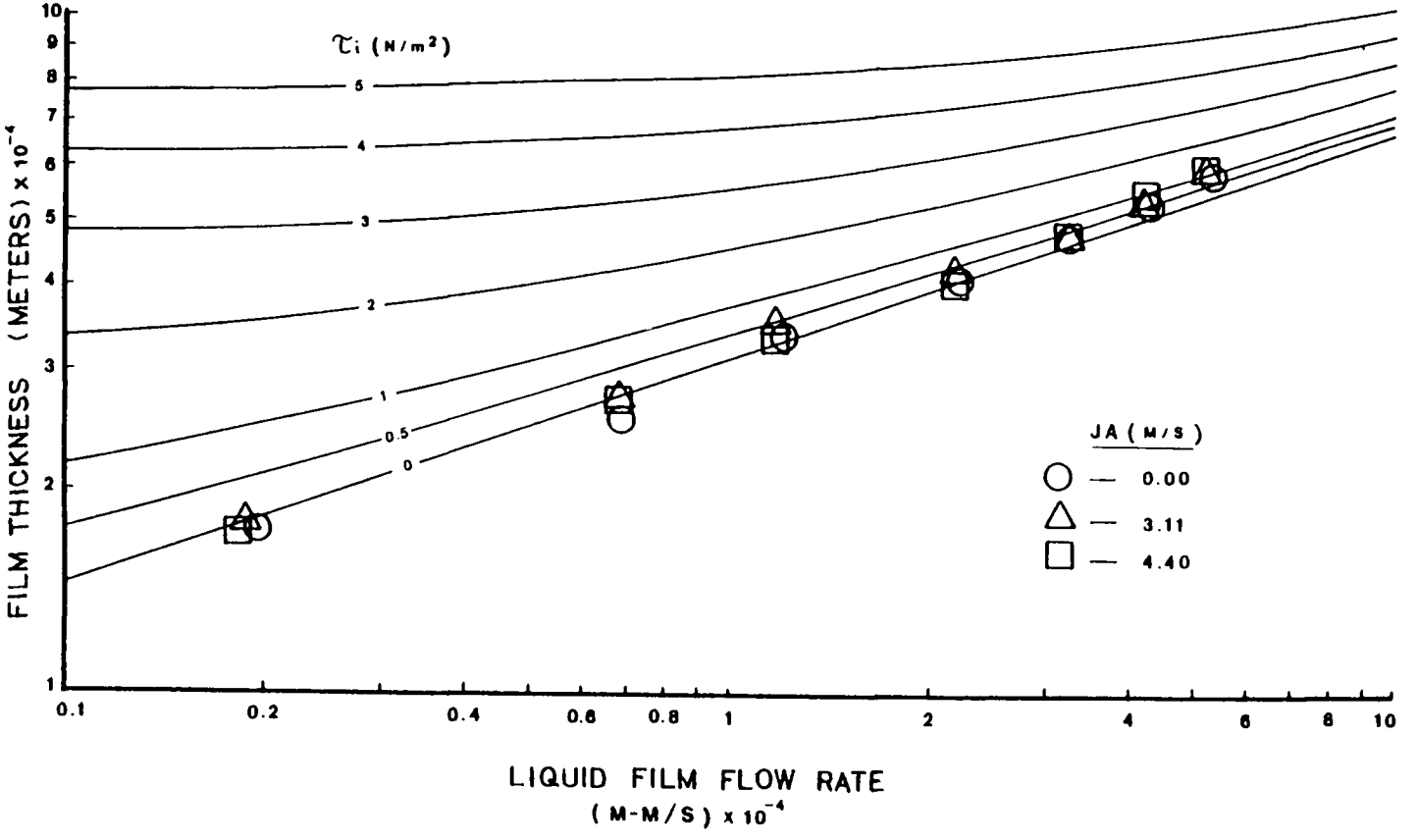

Figure 17. Effect of film flow rate upon film thickness for various interfacial shears

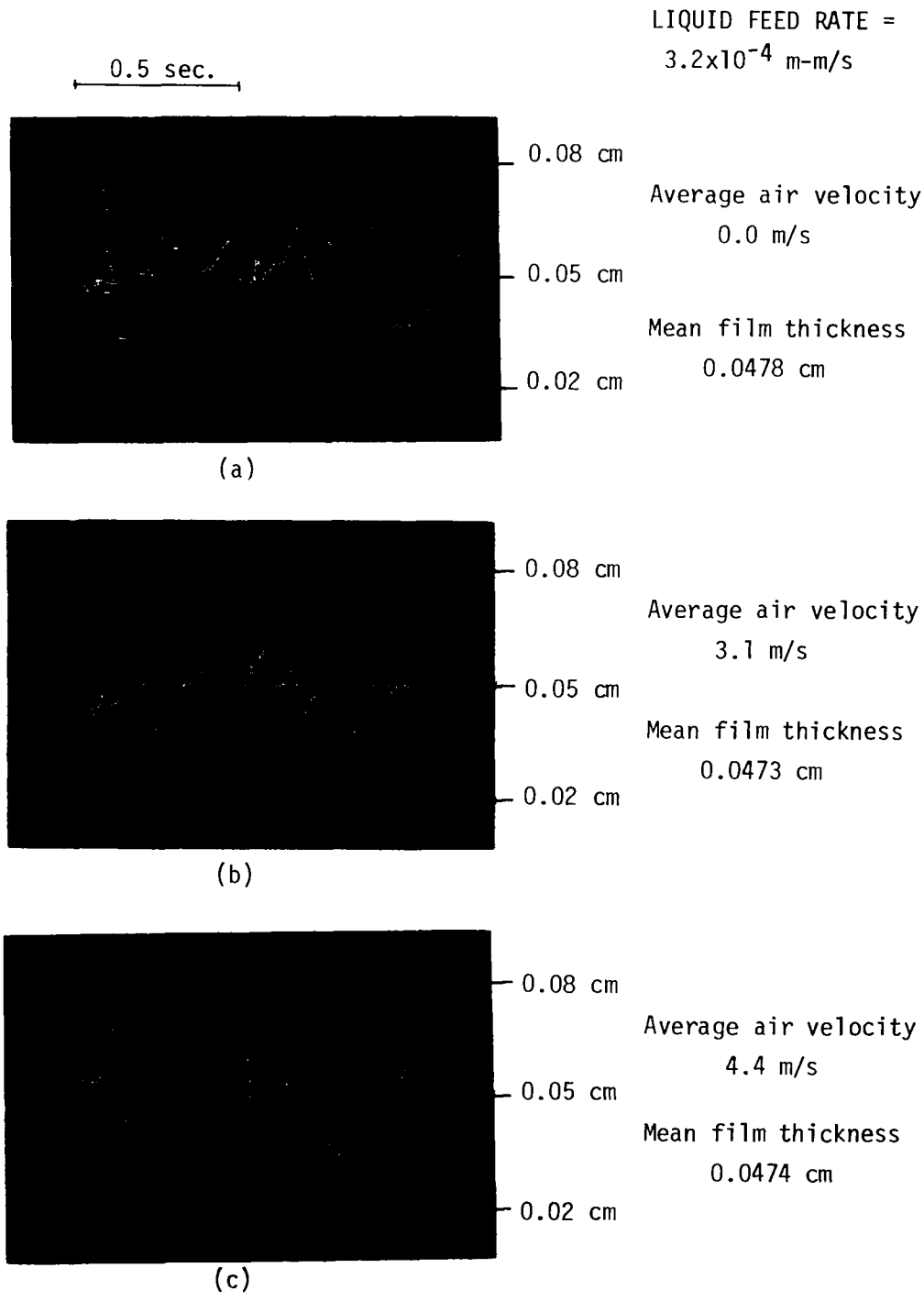

Figure 18. Interfacial profiles of constant liquid feed rate

LIQUID FEED RATE =
3.2×10^{-4} m-m/s

0.5 sec.

Average air velocity
5.4 m/s

Mean film thickness
0.0305 cm

(d)

Average air velocity
6.2 m/s

Mean film thickness
0.0187 cm

(e)

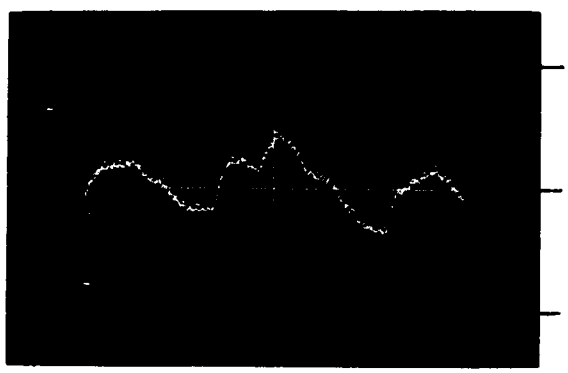

Average air velocity
7.0 m/s

Mean film thickness
0.0119 cm

(f)

FIGURE 18 cont.

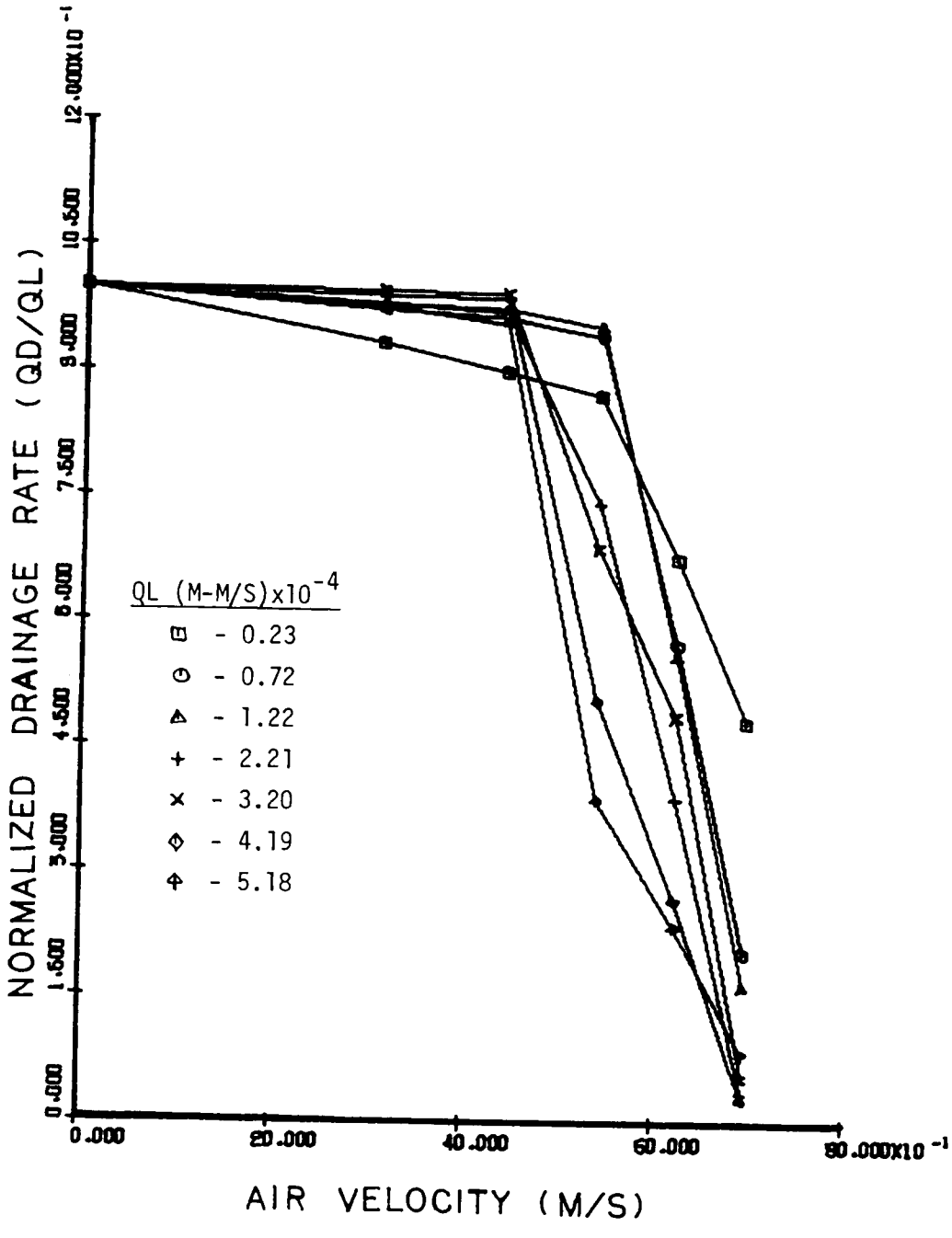

Figure 19. Effect of air flow upon normalized drainage rate

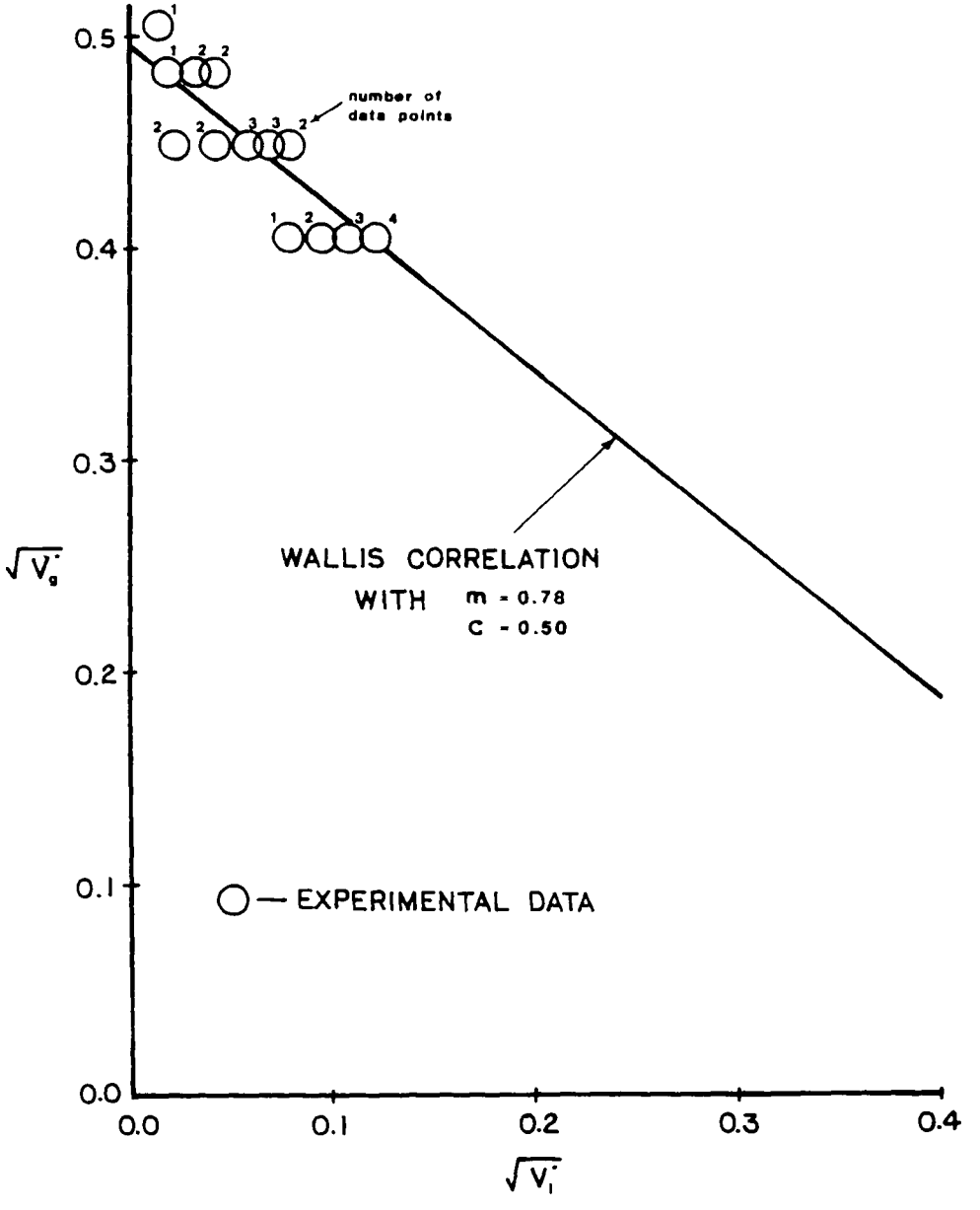

Figure 20. Wallis correlation for flooding

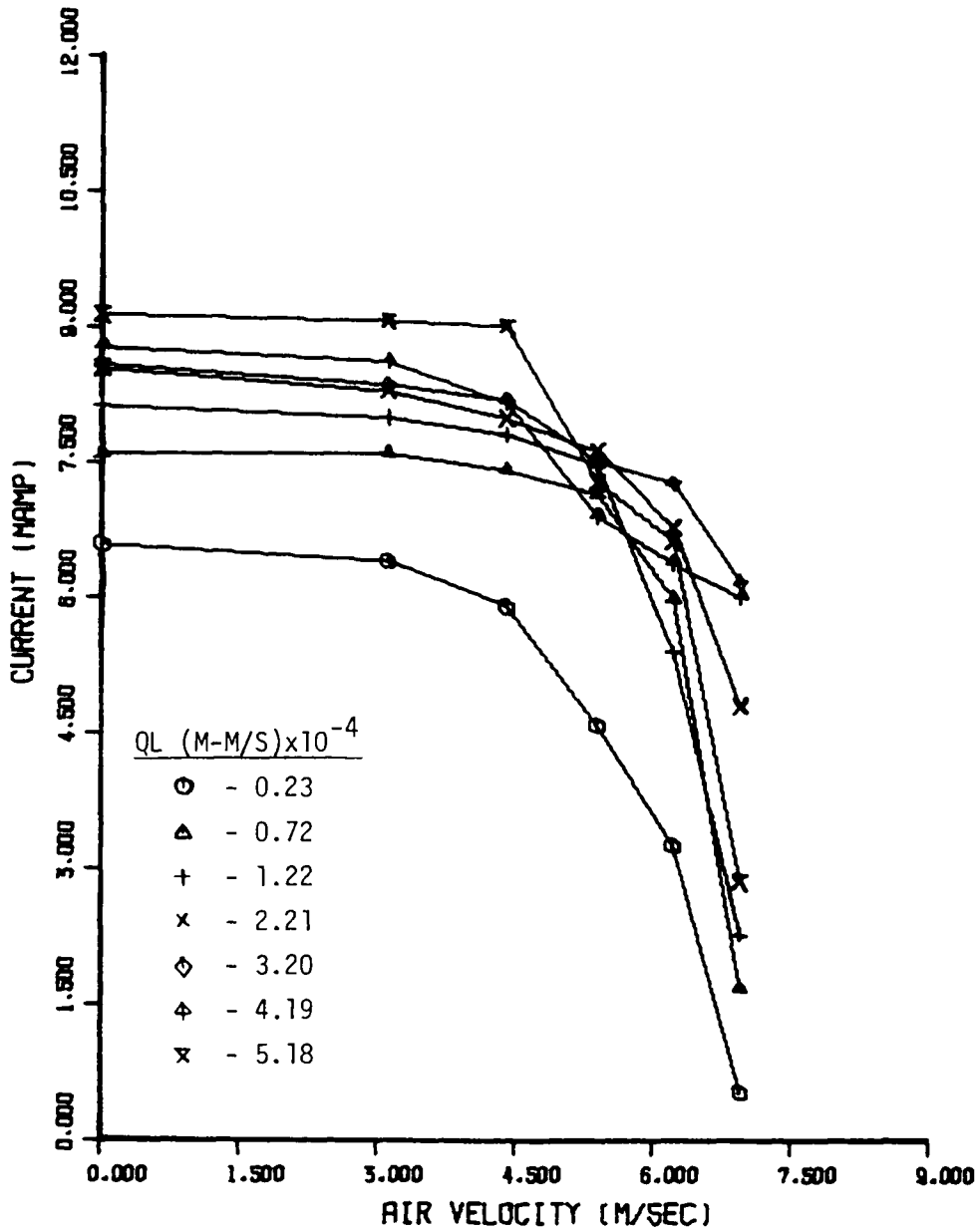

Figure 21. Electrolysis current as a function of air flow at constant liquid feed rates - Channel 1.

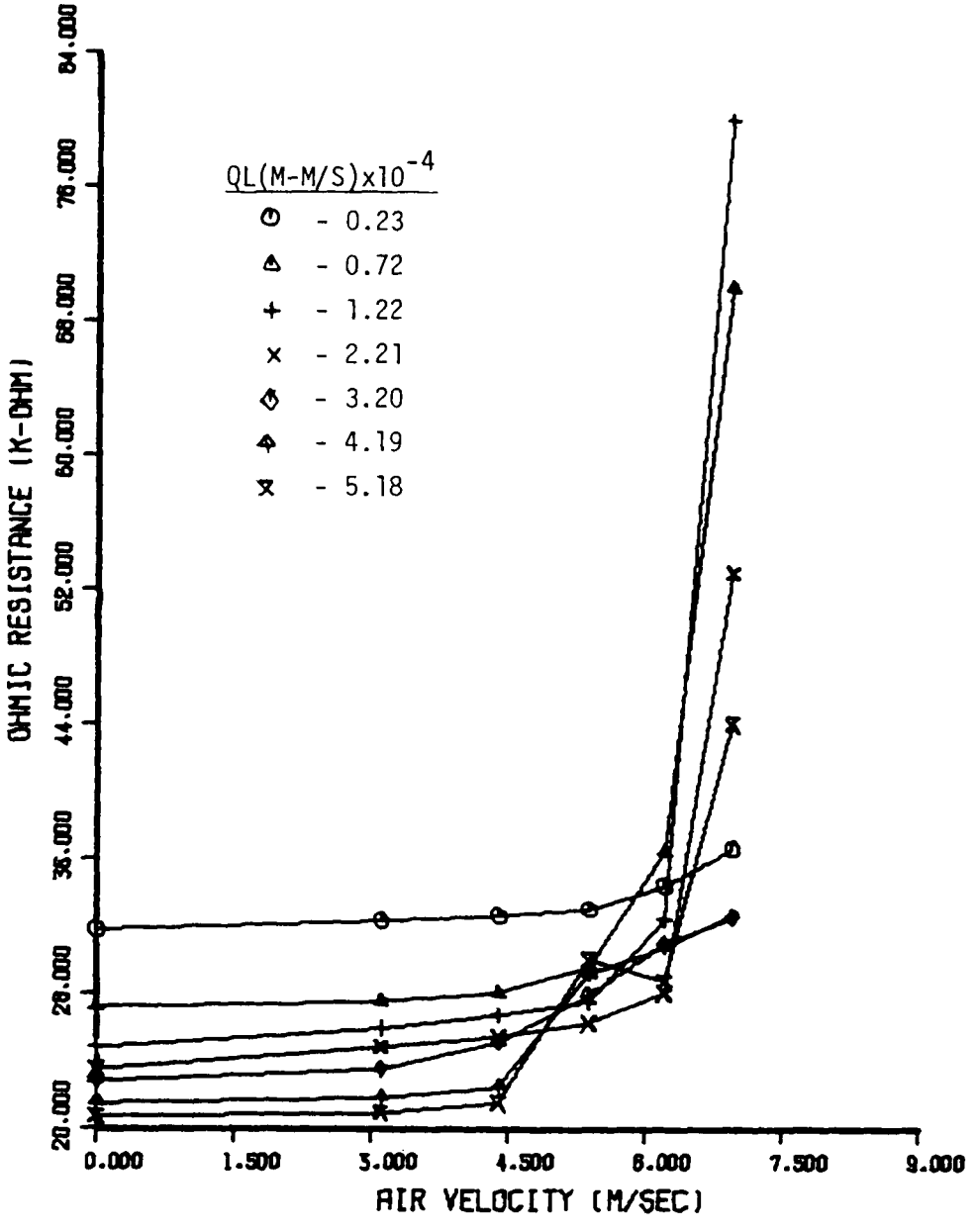

Figure 22. Ohmic resistance as a function of air flow at constant liquid feed rates - Channel 1.

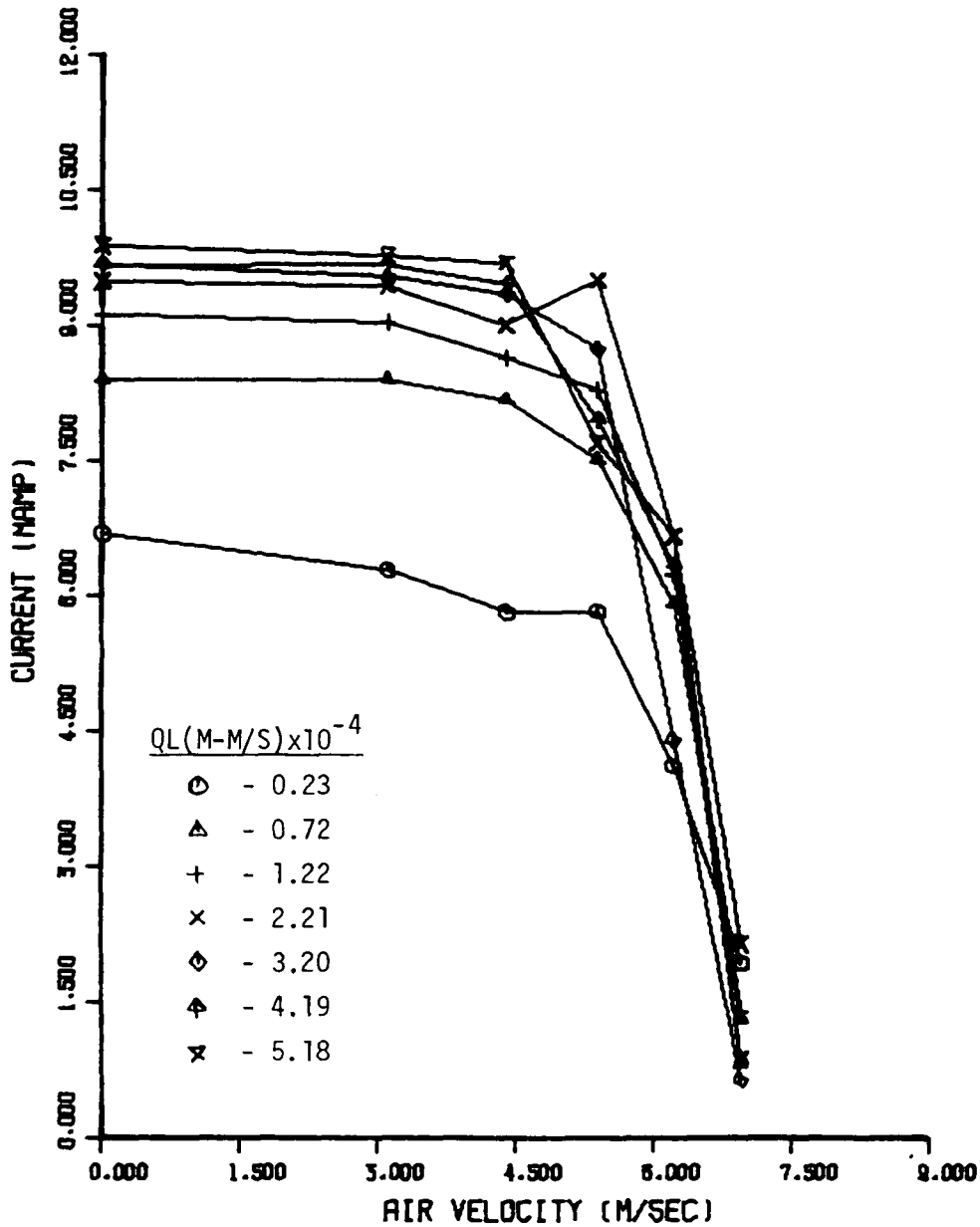

Figure 23. Electrolysis current as a function of air flow at constant liquid feed rates - Channel 2.

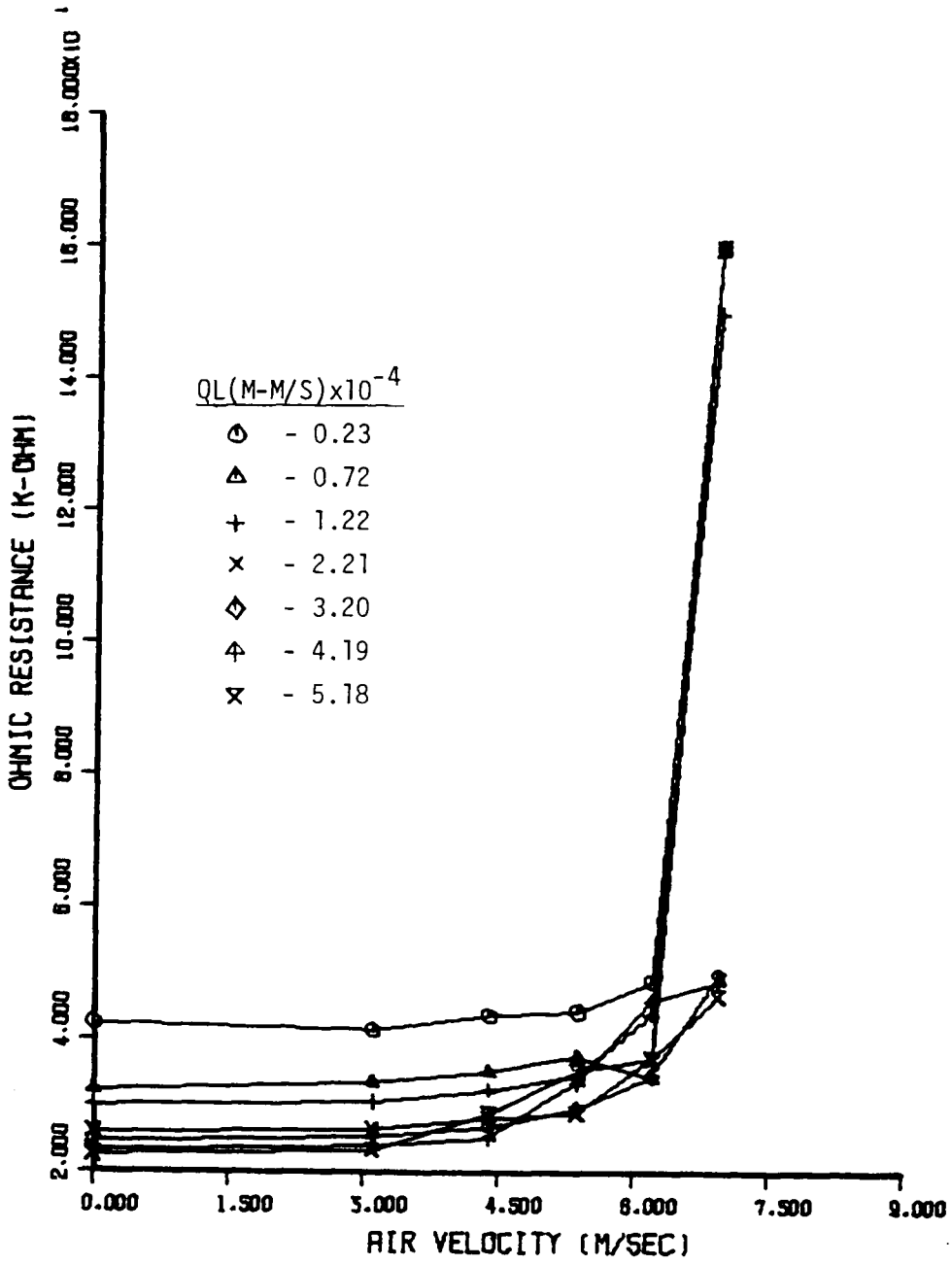

Figure 24. Ohmic resistance as a function of air flow at constant liquid feed rates - Channel 2.

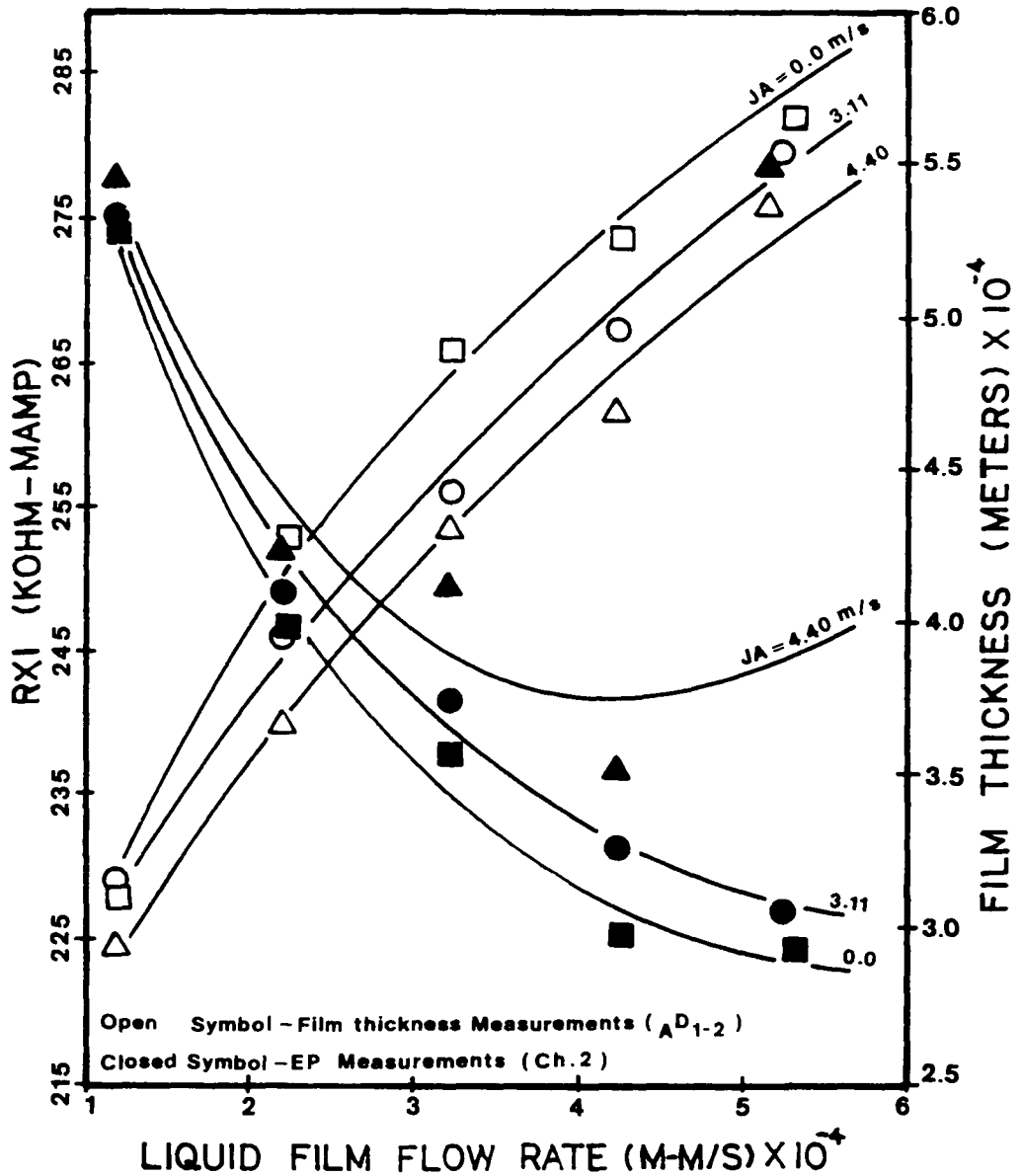

Figure 25. Effect of liquid film flow rate on product IxR_p and film thickness at constant air flows.

APPENDIX A

TABLE 1

BAND PROBES CALIBRATION

	D = 0.508 CM		D = 0.635 CM	
NO.	δ/d	$\Delta c/\Delta c_m$	δ/d	$\Delta c/\Delta c_m$
1	.18359	.27627	.14688	.21472
2	.20807	.31017	.16646	.25000
3	.23255	.34068	.18604	.27914
4	.25948	.37458	.20758	.30015
5	.27539	.40169	.22031	.31856
6	.30599	.43220	.24479	.34202
7	.32557	.45424	.26046	.36350
8	.35495	.47627	.28396	.38804
9	.37209	.50339	.29767	.40506
10	.40391	.52373	.32313	.42331
11	.42839	.55085	.34271	.44172
12	.45287	.57458	.36229	.45859
13	.47612	.59492	.38090	.47699
14	.50183	.62034	.40145	.49847
15	.52630	.63051	.42104	.51687
16	.55078	.65932	.44063	.53221
17	.57526	.66949	.46021	.54831
18	.58750	.69492	.47000	.55353
19	.61198	.71525	.48959	.56902
20	.67318	.75085	.53854	.60123
21	.73438	.77797	.58750	.63650
22	.79558	.81186	.63645	.66871
23	.85678	.84746	.68542	.69172
24	.91797	.86780	.73438	.72239
25	.97917	.88983	.78334	.74387
26	1.04037	.90169	.83230	.76840
27	1.10157	.91525	.88125	.78988
28	1.16277	.92881	.93021	.80828
29	1.22397	.94068	.97917	.82362
30	1.28516	.94746	1.02813	.83436
31	1.34636	.95593	1.07709	.84816
32	1.40756	.96271	1.12605	.86043
33	1.46876	.96949	1.17501	.87423
34	1.52996	.97627	1.22397	.88650
35	1.59115	.97966	1.27292	.89724

	D = 0.508 CM		D = 0.635 CM	
NO.	δ/d	$\Delta C/\Delta C_m$	δ/d	$\Delta C/\Delta C_m$
36	1.65235	.98136	1.32188	.90491
37	1.71355	.98475	1.37084	.91411
38	1.77475	.98475	1.41980	.92025
39	1.83595	.98814	1.46876	.92638
40	1.89715	.99153	1.51772	.93712
41	1.95834	.99322	1.56668	.94632
42	2.01954	.99492	1.61563	.94939
43	2.08074	.99661	1.66459	.95245
44	2.14194	.99661	1.71355	.96012
45	2.20314	.99831	1.76251	.96472
46	2.26434	.99831	1.81147	.96779
47	2.32553	.99831	1.86043	.97239
48	2.44793	.99831	1.95834	.98006
49	2.57033	1.00000	2.05626	.98313
50	3.05991	1.00000	2.44793	.99693
51	3.67190	1.00000	2.93752	1.00000

CALIBRATION EQUATION FOR THE 0.635 CM BAND PROBE -

$$Y = AX + BX^2 + CX^3$$

WHERE $Y = \delta/d$,

$X = \Delta C/\Delta C_m$,

A= 0.662404664023E+00
B=-0.182357117177E+00
C= 0.939365485897E+00

RANGE OF CAPACITANCE VALUES -

	DRY	THICK
0.508 CM	0.0 PF	59.0 PF
0.635 CM	0.0 PF	65.2 PF

TABLE 2

SPLID-D PROBES CALIBRATION

RUN NO.	Y .635 CM BAND	X ${}_{A}D_{1-2}$	X ${}_{A}D_{1-G}$	δ (METERS)
1	.051040	.416870	.082430	2.12465E-04
2	.088400	.535930	.127570	3.66906E-04
3	.102600	.631180	.161800	4.25816E-04
4	.116870	.661110	.186933	4.85292E-04
5	.127500	.702850	.204970	5.29839E-04
6	.134133	.756330	.230167	5.57761E-04
7	.143333	.797860	.259030	5.96672E-04
8	.155567	.827640	.284470	6.48790E-04
9	.163867	.869230	.306130	6.84422E-04

RUN NO.	Y .635 CM BAND	X ${}_{B}D_{3-4}$	X ${}_{B}D_{3-G}$	δ (METERS)
1	.051040	.388970	.086470	2.12465E-04
2	.088400	.549270	.143300	3.66906E-04
3	.102500	.611030	.169700	4.25816E-04
4	.116870	.660530	.187570	4.85292E-04
5	.127500	.709927	.205780	5.29839E-04
6	.134133	.746970	.223970	5.57761E-04
7	.143333	.777870	.249200	5.96672E-04
8	.155567	.827270	.285300	6.48790E-04
9	.163867	.870340	.310800	6.84422E-04

RANGE OF CAPACITANCE VALUES -

	DRY	THICK
BAND -	1.667 PF	66.933 PF
${}_{A}D_{1-2}$ -	1.967 PF	7.567 PF
${}_{A}D_{1-G}$ -	1.733 PF	11.100 PF
${}_{B}D_{3-4}$ -	2.300 PF	7.700 PF
${}_{B}D_{3-G}$ -	1.633 PF	10.967 PF

CALIBRATION EQUATION FOR THE SPLIT-D PROBES -

$$Y = AX + BX^2 + CX^3$$

FOR $_{A}D_{1-2}$

A=-0.130148920634E-01
B= 0.446034794049E+00
C=-0.248940726758E+00

FOR $_{A}D_{1-G}$

A= 0.712650653966E+00
B=-0.321788744172E+00
C=-0.910838558841E+00

FOR $_{B}D_{3-4}$

A= 0.217522059442E-01
B= 0.356767708865E+00
C=-0.189908674344E+00

FOR $_{B}D_{3-G}$

A= 0.520233469409E+00
B= 0.123656152868E+01
C=-0.395434165471E+01

WHERE $Y = \frac{\Delta C}{\Delta C_m}$ OF THE .635 CM BAND PROBE

$X = \frac{\Delta C}{\Delta C_m}$ OF THE SPLIT-D PROBES

TABLE 3

EFFECT OF AIR FLOW RATE ON FILM THICKNESS -
(.635 CM BAND PROBE)

	JA (M/S)	$\frac{\Delta C}{\Delta C_m}$	δ (METERS)
WATER RUN NO. 1		QL = 2.28253E-05	(M-M/S)
1	0.00000	4.17853E-02	1.74174E-04
2	3.10965	4.36460E-02	1.81877E-04
3	4.39770	4.10933E-02	1.71308E-04
4	5.38607	3.28446E-02	1.37116E-04
5	6.21929	2.64625E-02	1.10608E-04
6	6.95338	2.12560E-02	8.89425E-05
7	7.61705	8.80000E-03	3.69296E-05
WATER RUN NO. 2		QL = 7.23570E-05	(M-M/S)
1	0.00000	6.03668E-02	2.51011E-04
2	3.10965	6.59027E-02	2.73883E-04
3	4.39770	6.52671E-02	2.71257E-04
4	5.38607	6.34423E-02	2.63718E-04
5	6.21929	5.66863E-02	2.35803E-04
6	6.95338	1.95850E-02	8.19804E-05
7	7.61705	1.78775E-03	7.51611E-06
WATER RUN NO. 3		QL = 1.21889E-04	(M-M/S)
1	0.00000	8.07473E-02	3.35235E-04
2	3.10965	7.82635E-02	3.24964E-04
3	4.39770	7.66158E-02	3.18152E-04
4	5.38607	8.26132E-02	3.42953E-04
5	6.21929	4.76837E-02	1.98584E-04
6	6.95338	1.61119E-02	6.74955E-05
7	7.61705	2.21838E-03	9.32547E-06
WATER RUN NO. 4		QL = 2.20952E-04	(M-M/S)
1	0.00000	9.80934E-02	4.07095E-04
2	3.10965	9.85233E-02	4.08880E-04
3	4.39770	9.54689E-02	3.96204E-04
4	5.38607	9.30261E-02	3.86074E-04
5	6.21929	5.11401E-02	2.12878E-04
6	6.95338	2.38210E-02	9.96210E-05
7	7.61705	1.64426E-03	6.91310E-06

	JA (M/S)	$\frac{\Delta C}{\Delta C_m}$	δ (METERS)
WATER RUN NO. 5		QL = 3.20015E-04	(M-M/S)
1	0.00000	1.15170E-01	4.78189E-04
2	3.10965	1.13868E-01	4.72754E-04
3	4.39770	1.14168E-01	4.74006E-04
4	5.38607	7.33865E-02	3.04805E-04
5	6.21929	4.47839E-02	1.86587E-04
6	6.95338	2.85115E-02	1.19124E-04
7	7.61705	2.48337E-03	1.04387E-05
WATER RUN NO. 6		QL = 4.19079E-04	(M-M/S)
1	0.00000	1.28054E-01	5.32169E-04
2	3.10965	1.28746E-01	5.35078E-04
3	4.39770	1.34151E-01	5.57835E-04
4	5.38607	6.16555E-02	2.56336E-04
5	6.21929	5.19600E-02	2.16268E-04
6	6.95338	3.09440E-02	1.29227E-04
7	7.61705	6.33184E-03	2.65885E-05
WATER RUN NO. 7		QL = 5.18142E-04	(M-M/S)
1	0.00000	1.41202E-01	5.87641E-04
2	3.10965	1.43509E-01	5.97419E-04
3	4.39770	1.45486E-01	6.05813E-04
4	5.38607	6.11613E-02	2.54294E-04
5	6.21929	5.24816E-02	2.18425E-04
6	6.95338	3.06487E-02	1.28001E-04
7	7.61705	5.39633E-03	2.26656E-05
WATER RUN NO. 8		QL = 6.17205E-04	(M-M/S)
1	0.00000	1.55671E-01	6.49237E-04
2	3.10965	1.55965E-01	6.50493E-04
3	4.39770	1.59194E-01	6.64333E-04
4	5.38607	6.27759E-02	2.60965E-04
5	6.21929	5.70784E-02	2.37424E-04
6	6.95338	3.55573E-02	1.48368E-04
7	7.61705	6.85281E-03	2.87723E-05

TABLE 4

EFFECT OF AIR FLOW RATE ON FILM THICKNESS - (SPLIT-D PROBE, $_{A}D_{1-2}$)

	JA (M/S)	$\frac{\Delta C}{\Delta C_m}$	δ (METERS)
WATEP RUN NO. 1		QL = 2.28253E-05 (M-M/S)	
1	0.00000	3.32516E-01	1.48992E-03
2	3.10965	2.52402E-01	1.08382E-03
3	4.39770	2.49796E-01	1.07143E-03
4	5.38607	2.64167E-01	1.14031E-03
5	6.21929	2.68513E-01	1.16143E-03
6	6.95338	1.89036E-01	7.94051E-04
7	7.61705	1.21127E-01	5.03106E-04
WATER RUN NO. 2		QL = 7.23570E-05 (M-M/S)	
1	0.00000	4.54722E-01	2.23410E-03
2	3.10965	4.39918E-01	2.13415E-03
3	4.39770	4.42810E-01	2.15344E-03
4	5.38607	4.74134E-01	2.36981E-03
5	6.21929	4.05310E-01	1.91178E-03
6	6.95338	3.60229E-01	1.64379E-03
7	7.61705	3.03922E-01	1.33887E-03
WATER RUN NO. 3		QL = 1.21889E-04 (M-M/S)	
1	0.00000	5.04085E-01	2.59012E-03
2	3.10965	5.09199E-01	2.62913E-03
3	4.39770	4.87745E-01	2.46824E-03
4	5.38607	5.09918E-01	2.63464E-03
5	6.21929	5.62304E-01	3.05960E-03
6	6.95338	3.31324E-01	1.48347E-03
7	7.61705	1.90229E-01	7.99312E-04
WATER RUN NO. 4		QL = 2.20952E-04 (M-M/S)	
1	0.00000	6.16422E-01	3.54998E-03
2	3.10965	5.85784E-01	3.26562E-03
3	4.39770	5.58007E-01	3.02297E-03
4	5.38607	6.25359E-01	3.63638E-03
5	6.21929	5.21111E-01	2.72159E-03
6	6.95338	3.86650E-01	1.79804E-03
7	7.61705	2.58987E-01	1.11532E-03

	JA (M/S)	$\frac{\Delta C}{\Delta C_m}$	δ (METERS)
WATER RUN NO. 5		QL = 3.20015E-04 (M-M/S)	
1	0.00000	6.74771E-01	4.14367E-03
2	3.10965	6.30719E-01	3.68896E-03
3	4.39770	6.18464E-01	3.56959E-03
4	5.38607	6.19825E-01	3.58270E-03
5	6.21929	5.29616E-01	2.78902E-03
6	6.95338	5.02385E-01	2.57725E-03
7	7.61705	2.53889E-01	1.09090E-03
WATER RUN NO. 6		QL = 4.19079E-04 (M-M/S)	
1	0.00000	7.10376E-01	4.54200E-03
2	3.10965	6.81781E-01	4.21986E-03
3	4.39770	6.55572E-01	3.94047E-03
4	5.38607	5.38121E-01	2.85766E-03
5	6.21929	5.30637E-01	2.79720E-03
6	6.95338	5.51748E-01	2.97020E-03
7	7.61705	3.10049E-01	1.37062E-03
WATER RUN NO. 7		QL = 5.18142E-04 (M-M/S)	
1	0.00000	7.49183E-01	5.00958E-03
2	3.10965	7.37440E-01	4.86429E-03
3	4.39770	7.20588E-01	4.66159E-03
4	5.38607	5.32680E-01	2.81361E-03
5	6.21929	5.43235E-01	2.89952E-03
6	6.95338	5.31324E-01	2.80271E-03
7	7.61705	3.04216E-01	1.34039E-03
WATER RUN NO. 8		QL = 6.17205E-04 (M-M/S)	
1	0.00000	8.06203E-01	5.76412E-03
2	3.10965	7.74510E-01	5.33451E-03
3	4.39770	7.43056E-01	4.93336E-03
4	5.38607	5.29616E-01	2.78902E-03
5	6.21929	5.88644E-01	3.29141E-03
6	6.95338	5.47859E-01	2.93776E-03
7	7.61705	3.10049E-01	1.37062E-03

TABLE 5

EFFECT OF AIR FLOW RATE ON FILM THICKNESS - (SPLIT-D PROBE, $_{A}D_{1-6}$)

	JA (M/S)	$\frac{\Delta C}{\Delta C_m}$	δ (METERS)
WATER RUN NO. 1		QL = 2.28253E-05 (M-M/S)	
1	0.00000	6.25428E-02	2.60002E-04
2	3.10965	4.16087E-02	1.73442E-04
3	4.39770	2.36189E-02	9.87803E-05
4	5.38607	2.77869E-02	1.16113E-04
5	6.21929	1.62208E-02	6.79499E-05
6	6.95338	4.18892E-03	1.75999E-05
7	7.61705	1.40677E-03	5.91500E-06
WATER RUN NO. 2		QL = 7.23570E-05 (M-M/S)	
1	0.00000	1.00783E-01	4.18266E-04
2	3.10965	8.22618E-02	3.41500E-04
3	4.39770	8.22618E-02	3.41500E-04
4	5.38607	8.22618E-02	3.41500E-04
5	6.21929	8.41312E-02	3.49234E-04
6	6.95338	2.63006E-02	1.09935E-04
7	7.61705	2.35718E-03	9.90860E-06
WATER RUN NO. 3		QL = 1.21889E-04 (M-M/S)	
1	0.00000	1.23383E-01	5.12557E-04
2	3.10965	1.08897E-01	4.52023E-04
3	4.39770	1.06561E-01	4.42293E-04
4	5.38607	1.06000E-01	4.39958E-04
5	6.21929	1.09572E-01	4.54836E-04
6	6.95338	3.43194E-02	1.43234E-04
7	7.61705	3.75873E-03	1.57942E-05
WATER RUN NO. 4		QL = 2.20952E-04 (M-M/S)	
1	0.00000	1.44554E-01	6.01856E-04
2	3.10965	1.41139E-01	5.87373E-04
3	4.39770	1.38103E-01	5.74523E-04
4	5.38607	1.45863E-01	6.07413E-04
5	6.21929	2.40648E-02	1.00636E-04
6	6.95338	2.13288E-02	8.92456E-05
7	7.61705	5.10479E-03	2.14427E-05

	JA (M/S)	$\frac{\Delta C}{\Delta C_m}$	δ (METERS)
WATER RUN NO. 5		QL = 3.20015E-04	(M-M/S)
1	0.00000	1.78335E-01	7.47128E-04
2	3.10965	1.65713E-01	6.92377E-04
3	4.39770	1.60454E-01	6.69741E-04
4	5.38607	1.81071E-01	7.59080E-04
5	6.21929	4.16087E-02	1.73442E-04
6	6.95338	3.45759E-02	1.44298E-04
7	7.61705	6.41318E-03	2.69295E-05
WATER RUN NO. 6		QL = 4.19079E-04	(M-M/S)
1	0.00000	2.01886E-01	8.51072E-04
2	3.10965	1.94409E-01	8.17801E-04
3	4.39770	1.84440E-01	7.73840E-04
4	5.38607	1.64576E-01	6.87476E-04
5	6.21929	6.08713E-02	2.53096E-04
6	6.95338	5.55111E-02	2.30947E-04
7	7.61705	1.54410E-02	6.46950E-05
WATER RUN NO. 7		QL = 5.18142E-04	(M-M/S)
1	0.00000	2.26864E-01	9.64303E-04
2	3.10965	2.16606E-01	9.17392E-04
3	4.39770	2.16714E-01	9.17887E-04
4	5.38607	1.16623E-01	4.84260E-04
5	6.21929	4.92413E-02	2.05027E-04
6	6.95338	6.28705E-02	2.61355E-04
7	7.61705	1.76213E-02	7.37931E-05
WATER RUN NO. 8		QL = 6.17205E-04	(M-M/S)
1	0.00000	2.56838E-01	1.10500E-03
2	3.10965	2.58583E-01	1.11338E-03
3	4.39770	2.60016E-01	1.12027E-03
4	5.38607	1.18477E-01	4.92011E-04
5	6.21929	1.01794E-01	4.22467E-04
6	6.95338	8.72096E-02	3.61976E-04
7	7.61705	1.87120E-02	7.83413E-05

APPENDIX B

TABLE 6

DRAINAGE MEASUREMENTS

NO.	JA (M/S)	QD (M.M/S)	$\frac{QD}{QL}$
(1)	QL = 1.77495E-05 (M.M/S)		
1	0.00000	1.77495E-05	1.00000
2	3.10965	1.65636E-05	.93318
3	4.39770	1.59706E-05	.89978
4	5.38607	1.54765E-05	.87194
5	6.21929	1.20175E-05	.67706
6	6.95338	8.55851E-06	.48218
(2)	QL = 6.83495E-05 (M.M/S)		
1	0.00000	6.83495E-05	1.00000
2	3.10965	6.66298E-05	.97484
3	4.39770	6.60171E-05	.96588
4	5.38607	6.45347E-05	.94419
5	6.21929	3.93138E-05	.57519
6	6.95338	1.40731E-05	.20590
(3)	QL = 1.18949E-04 (M.M/S)		
1	0.00000	1.18949E-04	1.00000
2	3.10965	1.16676E-04	.98089
3	4.39770	1.16044E-04	.97557
4	5.38607	1.13573E-04	.95480
5	6.21929	6.65903E-05	.55982
6	6.95338	1.95877E-05	.16467
(4)	QL = 2.24814E-04 (M.M/S)		
1	0.00000	2.24814E-04	1.00000
2	3.10965	2.20663E-04	.98154
3	4.39770	2.18726E-04	.97292
4	5.38607	1.66921E-04	.74248
5	6.21929	8.76209E-05	.38975
6	6.95338	8.28179E-06	.03684

NO.	JA (M/S)	QD (M.M/S)	QD/QL
(5)	QL = 3.24452E-04 (M.M/S)		
1	0.00000	3.24452E-04	1.00000
2	3.10965	3.23504E-04	.99708
3	4.39770	3.22417E-04	.99373
4	5.38607	2.23391E-04	.68852
5	6.21929	1.58243E-04	.48772
6	6.95338	1.83029E-05	.05641
(6)	QL = 4.31088E-04 (M.M/S)		
1	0.00000	4.31088E-04	1.00000
2	3.10965	4.27510E-04	.99170
3	4.39770	4.26087E-04	.98840
4	5.38607	2.18192E-04	.50614
5	6.21929	1.15589E-04	.26813
6	6.95338	1.29465E-05	.03003
(7)	QL = 5.39581E-04 (M.M/S)		
1	0.00000	5.39581E-04	1.00000
2	3.10965	5.27682E-04	.97795
3	4.39770	5.16317E-04	.95688
4	5.38607	2.08725E-04	.38683
5	6.21929	1.26856E-04	.23510
6	6.95338	4.49470E-05	.08330

TABLE 7

OBSERVED FLOODING VELOCITIES

	.635 BAND		$_AD_{1-2}$	
	X	Y	X	Y
1	.0156	.5102	.0209	.4490
2	.0333	.4825	.0333	.4825
3	.0567	.4490	.0434	.4825
4	.0687	.4490	.0687	.4490
5	.0955	.4057	.0795	.4490
6	.1098	.4057	.0785	.4490
7	.1208	.4057	.1208	.4057

	$_AD_{1-G}$		ENTRAINMENT	
	X	Y	X	Y
1	.0184	.4825	.0209	.4490
2	.0427	.4490	.0427	.4490
3	.0434	.4825	.0567	.4490
4	.0687	.4490	.0786	.4057
5	.0795	.4490	.0955	.4057
6	.1098	.4057	.1098	.4057
7	.1208	.4057	.1208	.4057

WHERE $X = \sqrt{V_l^*}$

$Y = \sqrt{V_g^*}$

WALLIS FLOODING CORRELATION

$$Y = MX + C$$

WITH C = 0.4962860355
M = -.7822238845

AND THE AVERAGE DEVIATION OF THE DATA IS -
2.72785405 PERCENT

APPENDIX C

TABLE 8

FILM FLOW MEASUREMENTS

CHANNEL 1 (EP PROBE NO. 1)

WATER RUN	Q^c (M-M/S)	JA (M/S)	I (M-AMP)	R_p (K-OHM)
1	1.96194E-05	0.00000	6.58650	31.800
1	1.88704E-05	3.10965	6.40210	32.300
1	1.84959E-05	4.39770	5.98030	32.600
1	1.81963E-05	5.38607	4.58560	33.000
1	1.59991E-05	6.21929	3.25880	34.400
1	1.38259E-05	6.95338	.54106	36.600
2	6.98258E-05	0.00000	7.58830	27.200
2	6.87522E-05	3.10965	7.59970	27.500
2	6.83527E-05	4.39770	7.41700	28.000
2	6.74289E-05	5.38607	7.15420	29.500
2	5.14994E-05	6.21929	6.00030	36.400
2	3.55449E-05	6.95338	1.68780	70.000
3	1.20032E-04	0.00000	8.12430	24.800
3	1.18509E-04	3.10965	7.99320	25.900
3	1.18210E-04	4.39770	7.80250	26.700
3	1.16537E-04	5.38607	7.46930	27.500
3	8.69747E-05	6.21929	5.39970	32.400
3	5.72879E-05	6.95338	2.27690	80.000
4	2.23391E-04	0.00000	8.54040	23.500
4	2.20770E-04	3.10965	8.29410	24.800
4	2.19546E-04	4.39770	7.99320	25.400
4	1.86538E-04	5.38607	7.53480	26.200
4	1.36753E-04	6.21929	6.79580	28.000
4	8.66420E-05	6.95338	4.81100	53.000
5	3.22530E-04	0.00000	8.58510	22.800
5	3.22231E-04	3.10965	8.36190	23.500
5	3.21532E-04	4.39770	8.18730	25.100
5	2.58937E-04	5.38607	7.58820	27.900
5	2.56356E-04	6.21929	7.27530	31.000
5	1.29454E-04	6.95338	6.17710	32.500

WATER RUN	QF (M-M/S)	JA (M/S)	I (M-AMP)	R_p (K-OHM)
6	4.26664E-04	0.00000	8.77920	21.500
6	4.24417E-04	3.10965	8.62580	21.800
6	4.23518E-04	4.39770	8.16790	22.400
6	2.92211E-04	5.38607	6.91220	29.100
6	2.27395E-04	6.21929	6.39520	30.700
6	1.62578E-04	6.95338	6.01410	32.600
7	5.31695E-04	0.00000	9.13910	20.700
7	5.24180E-04	3.10965	9.06770	20.900
7	5.16989E-04	4.39770	9.01160	21.500
7	3.22714E-04	5.38607	7.28190	30.000
7	2.71006E-04	6.21929	6.63060	28.700
7	2.19272E-04	6.95338	2.86240	44.000

CHANNEL 2 (EP PROBE NO. 2)

WATER RUN	QF (M-M/S)	JA (M/S)	I (M-AMP)	R_p (K-OHM)
1	1.96194E-05	0.00000	6.68980	42.500
1	1.88704E-05	3.10965	6.28870	41.400
1	1.84959E-05	4.39770	5.82070	43.600
1	1.81963E-05	5.38607	5.83020	44.200
1	1.59991E-05	6.21929	4.11100	48.800
1	1.38269E-05	6.95338	1.94400	160.000
2	6.98258E-05	0.00000	8.40910	32.400
2	6.87522E-05	3.10965	8.40910	33.500
2	6.83527E-05	4.39770	8.17990	35.000
2	6.74289E-05	5.38607	7.52080	37.400
2	5.14994E-05	6.21929	5.91620	34.300
2	3.55449E-05	6.95338	1.32190	160.000

WATER RUN	QF (M-M/S)	JA (M/S)	I (M-AMP)	R_p (K-OHM)
3	1.20032E-04	0.00000	9.12550	30.100
3	1.18609E-04	3.10965	9.03950	30.500
3	1.18210E-04	4.39770	8.64550	32.200
3	1.16637E-04	5.38607	8.29450	34.600
3	8.69747E-05	6.21929	6.24210	43.800
3	5.72879E-05	6.95338	1.40310	150.000
4	2.23391E-04	0.00000	9.49800	26.000
4	2.20770E-04	3.10965	9.44780	26.400
4	2.19546E-04	4.39770	9.01080	28.000
4	1.86838E-04	5.38607	9.50750	28.800
4	1.36753E-04	6.21929	6.67750	37.000
4	8.66420E-05	6.95338	.86730	160.000
5	3.22830E-04	0.00000	9.67860	24.600
5	3.22231E-04	3.10965	9.55530	25.300
5	3.21532E-04	4.39770	9.35470	26.700
5	2.58987E-04	5.38607	8.74060	29.600
5	2.56366E-04	6.21929	4.40470	34.500
5	1.29454E-04	6.95338	.64090	49.900
6	4.26664E-04	0.00000	9.67470	23.300
6	4.24417E-04	3.10965	9.68660	23.900
6	4.23518E-04	4.39770	9.47500	25.000
6	2.92211E-04	5.38607	7.95540	33.400
6	2.27395E-04	6.21929	6.34120	45.800
6	1.62578E-04	6.95338	.84440	48.700
7	5.31695E-04	0.00000	9.88950	22.700
7	5.24180E-04	3.10965	9.78450	23.200
7	5.16989E-04	4.39770	9.69860	28.800
7	3.22714E-04	5.38607	7.69270	35.300
7	2.71006E-04	6.21929	6.66120	37.200
7	2.19272E-04	6.95338	2.14610	46.600

VITA

The son of Mr. and Mrs. Chok-Ching Lau, Tak-Oi Lau, was born on October 6, 1953, in Kowloon, Hong Kong. He attended high school in Hong Kong, and graduated in 1974. In the fall of that year, he entered University of Lowell and received a Bachelor of Science degree in Mechanical Engineering in June of 1978.

He entered Lehigh University in September 1978 as a graduate student in the Department of Mechanical Engineering.